Master thesis

Model for Mechanical Properties of Hot-Rolled Steels

Ryu, Joo Hyun (柳朱炫)

Department of Ferrous Technology

(Computational Metallurgy)

Graduate Institute of Ferrous Technology

Pohang University of Science and Technology

2008

Model for Mechanical Properties of Hot-Rolled Steels

2008

Ryu, Joo Hyun

열연강의 기계적 성질 모델

Model for Mechanical Properties
of Hot-Rolled Steels

Model for Mechanical Properties
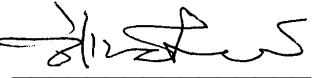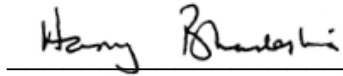# of Hot-Rolled Steels

By

Ryu, Joo Hyun
Department of Ferrous Technology
(Computational Metallurgy)
Graduate Institute of Ferrous Technology
Pohang University of Science and Technology

A thesis submitted to the faculty of Pohang University of Science and Technology in partial fulfillments of the requirements for the degree of Master of Science in the Graduate Institute of Ferrous Technology (Computational Metallurgy)

Pohang, Korea
December 20th, 2007

Approved by

Prof. Lee, Hae Geon   Prof. Bhadeshia, H.K.D.H.

_____   _____
Major Advisor   Co-Advisor

1

Model for Mechanical Properties
of Hot-Rolled Steels

Ryu, Joo Hyun

This dissertation is submitted for the degree of Master of Science at the Graduate Institute of Ferrous Technology of Pohang University of Science and Technology. The research reported herein was approved by the committee of Thesis Appraisal

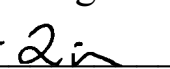December 20th, 2007

Thesis Review Committee

Chairman: Prof. Lee, Hae Geon

(Signature)_____

Member: Prof. Kim, In Gee

(Signature)_____

Member: Prof. Qin, Rong Shan

(Signature)_____

Member: Prof. Gaye, Henri R.

(Signature)_____

MFT   Ryu, Joo Hyun
20062868   Model for Mechanical Properties of
             Hot-Rolled Steels, Department of Ferrous Technology
             (Computational Metallurgy) 2007
             Adivisor: Prof. Lee, Hae Geon; Prof. Bhadeshia, H.K.D.H.
             Text in English

Abstract

The objective of this work was to produce the neural network models to capture and understand the relationship between the variables and mechanical properties of the hot-rolled steels. There are many factors that affect mechanical properties during the process.

Several neural network models have been developed for the ultimate tensile strength, yield strength and elongation as a function of chemical elements and thermo-mechanical variables to deal with complexity and uncertainty. The models were used to interpret trends by altering one variable and keeping other contents constant. Such studies are often not possible to conduct experimentally. The comparisons between the models confirm that the predictive power of models increases by adding relevant variables and data. In addition, the predictions of the neural network models are much more consistent with the published data in spite of rather big modeling uncertainties, when compared with linear models produced in this work.

Contents

Nomenclature

A_0	Original cross-sectional area of tensile test specimen
A	Instantaneous cross-sectional area of tensile test specimen
C_t	Coil thickness
E	Young's modulus
E_D	Error function in neural networks
E_w	Regularisation function in neural networks
F	Force
F_R	Driving force for recrystallization
K	Fitting parameter on the true stress-strain curve
L_0	Original length of tensile test specimen
L	Instantaneous length of tensile test specimen
L_l	Mean lineal intercept length
M	Magnification
M_w	Objective function of neural networks
N_l	Number of intercepts
L_T	Total length of the test lines
P	Total number of grain boundary intersections and
T_C	Coiling temperature
T_{FR}	Finish-rolling temperature
T_{nr}	Non recrystallization temperature
T_R	Slab reheating temperature
W	Content of chemical elements in weight percent
b	Burgers vector
d_α	Ferrite grain sizes
k_y	Dislocation locking parameter or grain boundary hardening coefficient
n	Work hardening exponent

t_R	Slab reheating time
x_j	Input variables in neural networks
x_{max}	Maximum values in database
x_{min}	Minimum value in the database
x_N	Normalized value
y	Output in neural networks
w_i	Weights in neural networks
α	Hyperparameter in neural networks
β	Hyperparameter in neural networks
γ	Austenite
ε_r	Total reduction ratio of finishing rolling
ε_T	True strain
$\mathcal{E}$	Percent elongation
ε	Engineering strain
σ	Engineering stress
σ_U	Ultimate tensile strength
σ_T	True stress
σ_Y	Yield strength
$\sigma_{Y_{0.2}}$	0.2% proof stress
σ_0	lattice friction stress
σ_w	Weight variance in neural networks
σ_v	Perceived level of noise in neural networks
μ	Shear modulus
ρ	Dislocation density
$\Delta\tau$	Change in critical resolved shear stress
Λ	Particle spacing
θ_j	Biases in neural networks

Ⅰ **Literature Review**

Introduction

Hot rolled strips and plates occupy a large proportion of the total annual steel production in the world. A modern hot-strip mill can produce more than 6 million tons of steel per annum. The most attractive property of the hot rolling process is its ability to produce large quantities of product in a reliable manner at an attractive cost. The process and product can nevertheless stand further optimization.

Hot rolling is generally conducted at a temperature greater than that at which the austenite recrystallizes as the continuously-cast slab is reduced to its final thickness in the range 1.2-22.0 mm. The mechanical properties of the steel are affected by the thermo-mechanical processing parameters, chemical composition and heat-treatment. It would be desirable to create a relationship between the mechanical properties and controlling variables.

Many researchers have expressed trends between the variables using linear regression equations [Jaiswal and McIvor, 1989], but such methods require the prior assumption of a relationship, are linear or pseudo-linear and are not sufficiently flexible to capture the complexity in the data. Neural networks are ideal in these circumstances and are able to deal with intricate problems. Neural networks are non-linear models used for empirical regression and their flexibility makes them able to capture complicated relationships in data. There are many examples of neural networks applied to the modeling of steel properties [Warde and Knowles, 1999; Jianlin, 2007]. There are also previous studies researching the mechanical properties of hot-rolled strip [Nolle et al., 1999; Andorfer, 2006]. Furthermore, the neural network can be applied for a

1

hot rolling process operating system at high automation levels [Martin et al., 1999]. Nevertheless, they have not taken modeling uncertainties into account.

This work here uses the neural networks with a Bayesian framework [MacKay, 1995]. The Bayesian approach to neural networks makes predictions with an uncertainty which dependents on a position in the input space. This is extremely meaningful for an exploration of new composition of steel [Bhadeshia, 2006].

1.1 Mechanical Property

1.1.1 Tensile Test

A tensile test is widely used to provide key information on the strength of materials. A specimen is tested to an increasing uniaxial tensile force at uniform speed with the simultaneous observation of elongation of the specimen. When the force is applied to the specimen, deformation occurs. If the deformation is immediately recovered after the force is terminated, it is elastic. The elastic deformation is related to a stretching of bonds in materials. Engineering stress (σ) is the force (F) per unit original cross-sectional area (A_0) of the specimen [Dieter, 1988]:

$$\sigma = \frac{F}{A_0} \hspace{3cm} (1\text{-}1)$$

Engineering strain (ε) is the elongation per unit original length (L_0) of the specimen.

$$\varepsilon = \frac{(L-L_0)}{L_0} \hspace{3cm} (1\text{-}2)$$

where L is instantaneous length of specimen.

The stress and elastic strain are directly proportional in the elastic region and related by the Young's modulus which is associated to the potential energy of the interatomic bonds. Hooke's law is an expression of this relationship:

$$\sigma = E\varepsilon \qquad\qquad (1\text{-}3)$$

where E is the Young's modulus [Dieter, 1988].

A permanent deformation which follows elastic strain is called plastic. If a straight line is drawn from the origin along the elastic behavior, the point at which the line deviates corresponds to the beginning of the plastic deformation. This is the yield point and the stress necessary to initiate macroscopic plasticity is the yield strength (σ_Y) of the material [Figure 1.1]. However, the detailed nature of the yield point is sensitive to the structure of the materials. Some materials show a distinct point, whereas others exhibit a slow change in the slope at the elastic range. In the case of the latter, the yield strength is conventionally defined as the proof stress ($\sigma_{Y_{0.2}}$), by finding the intersection of the stress-strain curve with a line parallel to the elastic slope of the curve and which intercepts the abscissa at 0.2% of the strain.

The maximum stress on the engineering stress-strain curve is known as the ultimate tensile strength σ_U, at which point the deformation becomes localized as the cross sectional area rapidly decreases compared with the remaining parts. The stress to continue to deform the specimen falls off, and this phenomenon is called necking [Felbeck and Atkins, 1984]. When the necking becomes substantial, the stress begins to decreases because the engineering stress and strain are calculated assuming the original cross-sectional area before the onset of necking. However, the stress to produce further deformation should increase locally at the neck because the metal continues to work-harden up to the point of fracture.
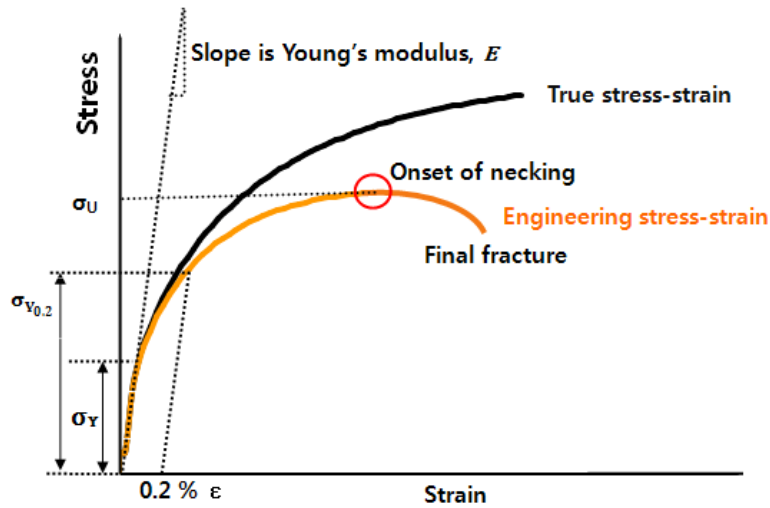
Figure 1.1 Characteristics of the stress-strain curve.

1.1.2 Work-hardening

The true stress (σ_T) and strain (ε_T) are determined from the instantaneous cross-sectional area (A) during the tensile test (Equation 1-4 and 5) and most the true stress-strain curves fit a simple power law expression by Holloman:

$$\sigma_T = \frac{F}{A} = \frac{FL}{A_0 L_0} = \frac{F}{A_0}\left(\frac{L-L_0+L_0}{L_0}\right) = \sigma(1+\varepsilon) \qquad (1\text{-}4)$$

$$\varepsilon_T = \ln\frac{L}{L_0} = \ln\left(\frac{L-L_0+L_0}{L_0}\right) = \ln(1+\varepsilon) \qquad (1\text{-}5)$$

$$\sigma_T = K\varepsilon_T^n \qquad (1\text{-}6)$$

where n used to characterize the stress-strain behavior (Equation 1-7) is the work hardening exponent and K is the fitting parameter on that curve.

$$n = \frac{d(\ln\sigma_T)}{d(\ln\varepsilon_T)} = \frac{\varepsilon_T}{\sigma_T}\frac{d\sigma_T}{d\varepsilon_T} \qquad (1\text{-}7)$$

4

The plastic deformation in ductile materials requires higher stresses because the dislocations defined as irregularities in a crystal structure multiply during the extension and their motion becomes more difficult because of the enhanced interactions among them, leading to working-hardening. The plastic deformation not only moves existing dislocations but also produces a great number of new dislocations. The increase in strength ($\Delta\sigma$) due to the interaction of dislocations was derived by Taylor [1934]:

$$\Delta\sigma = a\mu b(\rho^{\frac{1}{2}}) \tag{1-8}$$

where μ is the shear modulus, a is a constant approximately equal to 0.5 in the theory b is the magnitude of the Burgers vector and ρ is the dislocation density.

If the dislocation motion and plastic deformation have been hindered by the dislocation accumulation, and elastic deformation has reached its limit, fracture occurs.

1.1.3 Grain Size Hardening

The generated dislocations pile up on grain boundaries which present slip discontinuities. The stress, therefore, has to increase forcing the dislocations closer together until eventually dislocation motion is triggered in adjacent grains [Honeycombe, 1981].

The yield strength varies as a function of the ferrite grain size$^{-\frac{1}{2}}$ (d_α) in a range 6 to 30 μm, according to the Hall-Petch equation:

$$\sigma_Y = \sigma_0 + k_y d_\alpha^{-1/2} \tag{1-9}$$

where σ_0 = the *lattice friction stress*, and is the yield stress for the limit $L\rightarrow\infty$, and k_y = the slope of the line and is known as the *dislocation locking parameter*, which represents the relative hardening contribution due to grain boundaries.

The validity of the Hall-Petch relationship has been confirmed for grain sizes in the range 1.5 to 150 μm for ferritic steels [Morrison, 1966]

Grain size also has an effect on the work-hardening rate and therefore the ultimate tensile strength. Work hardening takes place within the grains during plastic deformation and Morrison has shown that the work-hardening exponent *(n)* depends on the grain size *(d)* [Morrison, 1966]:

$$n = 5 \, / \, (10 + d_\alpha^{-\frac{1}{2}}) \qquad\qquad (1\text{-}10)$$

The most general method for measuring the grain size is the mean lineal intercept method using test lines [Richard, 1994]. The mean lineal intercept length (L_l) is determined by laying a series of test lines on planar sections and counting the number of times that grain boundaries are intercepted:

$$L_l = \frac{1}{N_l} = \frac{L_T}{PM} \qquad\qquad (1\text{-}11)$$

where N_l is the number of intercepts per total length of the test lines, L_T, P is the total number of grain boundary intersections and *M* is the magnification.

1.1.4 Solid Solution Hardening

Solid solution strengthening occurs because the differences between the solute and solvent atoms interfere with dislocations as they move through the lattice. Two types of solid solution strengthening can occur depending on the size of the alloying element. Substitutional solid solution strengthening occurs when the solute atom is large enough to replace the solvent atoms in their lattice positions. The solvent and solute atoms must differ in atomic size by less than 15% to obtain solubility, according to the Hume-Rothery rules [Honeycombe, 1968]. Interstitial solid solution occurs when the solute atoms are less than half as small as the solvent atoms [Felbeck and Atkins, 1984]. Carbon is always in interstitial solid solution in iron.

Solid solution strengthening with solutes of higher shear modulus achieves noticeable strengthening. Both the higher shear modulus and very different lattice parameters increase stiffness and introduce local stress fields. Dislocation propagation will be hindered at these sites, impeding plasticity and increasing the yield strength proportionally with solute concentration [Cottrell, 1953].

1.1.5 Precipitation Hardening

C and N retained in solid solution due to rapid cooling can be precipitated as carbides or nitrides respectively during processing. In microalloyed steels, strengthening is achieved by a dispersion of small carbides or nitrides of Ti, Nb and V, and the formation of these precipitates depends a lot on the heat treatment and rolling process. The interaction between the precipitates and the dislocations during plastic deformation is responsible for the strengthening [Gladman, 1997].

The precipitates may have a different crystal structure from that of the surrounding ferrite. Once plastic deformation occurs, additional energy is needed either to increase the length of the dislocation line as the dislocation bypasses the particles or to create new particle interface with the surrounding matrix as the dislocation passes through the precipitates. Orowan has shown that particle size and spacing are important aspects of precipitation strengthening [Honeycombe, 1968].

$$\Delta\tau = \frac{a \cdot \mu \cdot b}{\Lambda} \qquad\qquad (1\text{-}12)$$

where $\Delta\tau$ is the increase in critical resolved shear stress caused by the particles with a spacing (Λ), a is a constant about ~0.5, b the magnitude of the Burgers vector and μ is the shear modulus.

8

1.2 Hot Rolling Process

A hot strip mill consists of, from start to finish, reheat furnaces, roughing mill, finishing mill, runout table with accelerated cooling and finally a coiler, as shown in Figure 1.2. The evolution of microstructure during processing is dependent on the chemical composition, the finish-rolling temperature (T_{FR}), coiling temperature (T_C), reheating temperature (T_R), reheating time (t_R), total reduction ratio (ε_r) of finishing rolling and coil thickness (C_t). Slabs approximately 220×650×1650 mm in size are rolled into strips of thickness in the range 1.6 – 22 mm, and during this operation they cool down to room temperature from about 1200 ℃. Figures 1.3 and 4 show the change of thickness and temperature of 100 steels in the dataset exploited in this work. Work hardening and dynamic recovery occur simultaneously, and the accumulated energy due to defects created in the steel is the driving force for recovering and recrystallization. These microstructural phenomena associated with the deformation of austenite have been investigated for several decades [Hodgson, 1993; Medina, 1996; Ouchi et al., 1977].
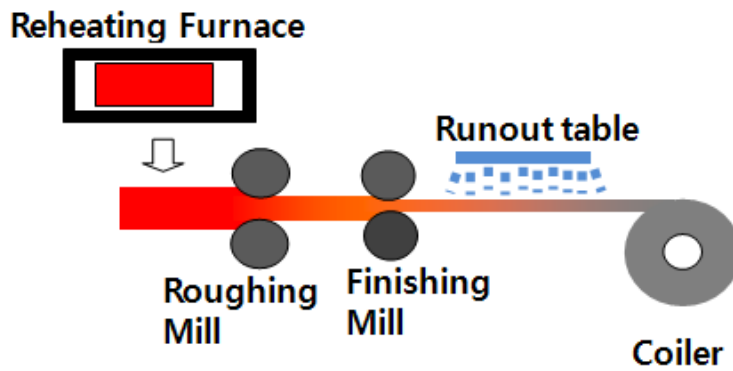

Figure 1.2 Hot rolling process consists of reheating furnace, roughing mill, finishing mill, runout table and coiler.
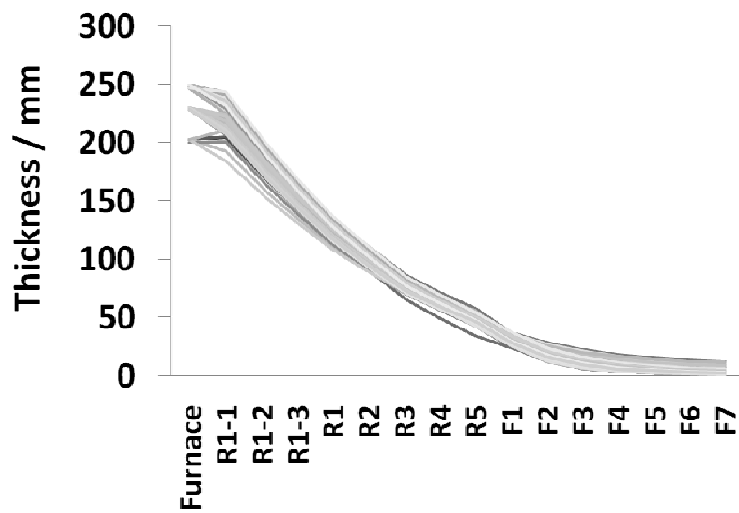
Figure 1.3 Change of thickness of steel during working process which consists of reheating furnace, roughing mill (R1-R5) and finishing mill (F1-F7), as used in this work.
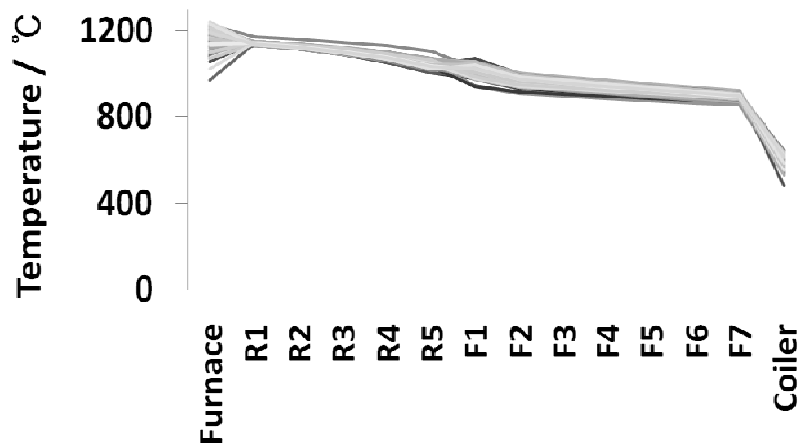

Figure 1.4 Change of temperature from reheating furnace to coiler in this work. Steels are cooled down to room temperature in a variety of ways to achieve the appropriate final microstructure after coiling.

1.2.1 Reheating Furnace

In the reheating furnaces the slabs are heated up to 1100 – 1200 ℃ and the resulting coarse austenite is in a fully annealed state with a low defect density (Figure 1.5). The temperature of the slab is essentially homogeneous. The reheating temperature and time influences the γ grain size and there is some homogenization of the chemical segregation associated with the solidification microstructure. In all microstructures, the carbon is in solid solution in the austenite at 1100 ℃, apart from minute quantities tied up with precipitated microalloying elements.
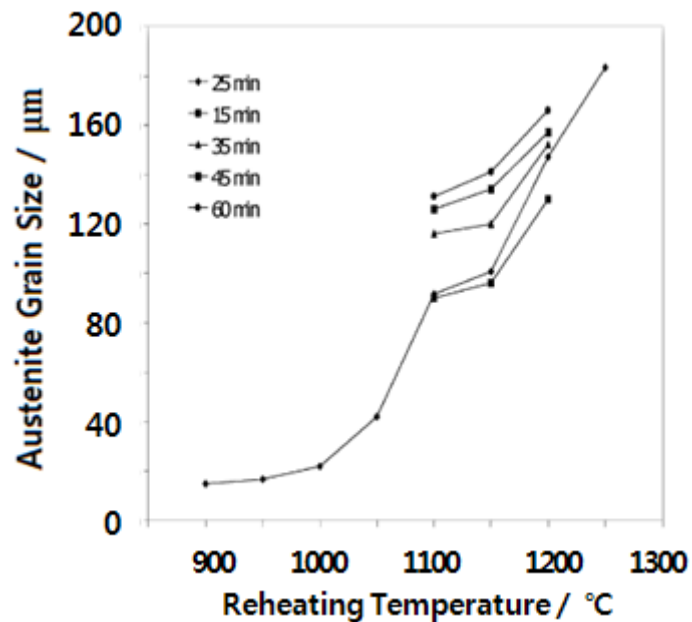

Figure 1.5 Dependence between reheating temperature, time and average austenite grain size of Fe-0.1C-0.9Mn-0.007N-0.011P-0.008S-0.04Al-0.03Nb-0.04Ti-0.03Cu-0.01Si-0.003V steel [Zrnik et al., 2003].

In microalloyed steels, precipitates such as TiN and Nb(CN) can inhibit austenite grain growth via Zener Pinning. Such precipitates many remain undissolved below 1250 ℃ and 1150 ℃ respectively [Cuddy, 1985]. Similarly, the dissolution of other pinning precipitates, particularly AlN, VC and VN, is also time and temperature dependent (Figure 1.6) [Eastering, 1992]. The greatest effect of Zener pinning is shown for TiN (Figure 1.7).
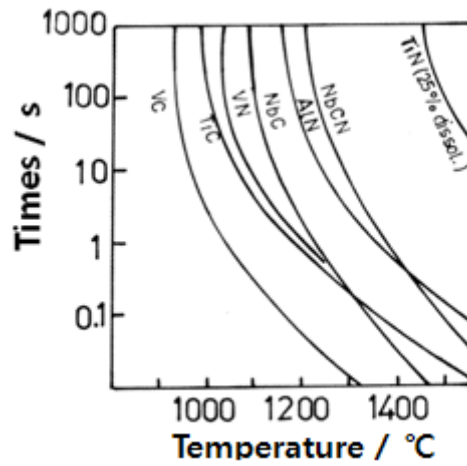

Figure 1.6 Dissolution kinetics of precipitates [Eastering, 1992].
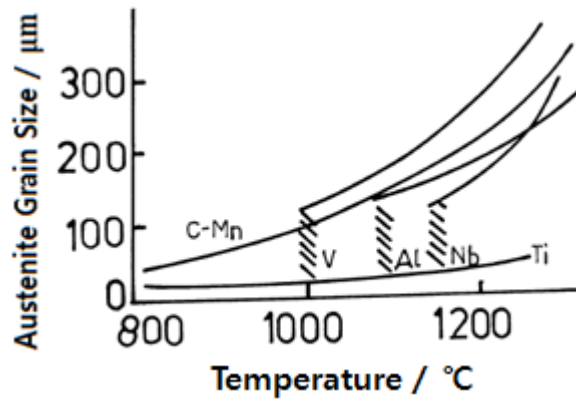

Figure 1.7 Effect of reheating temperature and microalloying on austenite grain size. Ti is the most effective in retarding grain growth at elavated temperatres [Cuddy, 1985].

12

1.2.2 Roughing Mill

The heated slabs are rolled in roughing mill to intermediate thickness in the range 60-150 mm. In the roughing mill, the time between rolling stands is relatively long and the temperature is high, so full recrystallization occurs in this stage. Due to the high temperature (1050 - 1150 ℃), the rather low strain rate (<10 s^{-1}) and the large strains (0.4 - 0.6) there is also a possiblilty for dynamic recrystallization to occur during deformation. Recrystallization means the formation of a new grain structure in a deformed material, induced by the need to reduce the stored energy of deformation [Doherty et al., 1997]. The average recrystallized grain size decreases with increasing deformation. Fine grains are desirable as they contribute to high strength and toughness.

1.2.3 Recovery, Recrystallization and Microalloying

Thremomechanical processing includes the control of reheating temperature, reduction rate, finishing rolling temperature, cooling rate and coiling temperture. The purpose is to obtain an optimum ferrite grain size. There are different ways of achieving this and the control of T_{FR} is an important factor. When the austenite is deformed, its dislocation density increases and so does the amount of grain surface per unit volume [Tamura et al., 1988; Zhu et al., 2007]. As a result, processes such as dynamic recovery, recrystallization, static recovery and recrystallization occur in order to reduce the stored energy. Recovery is an annihilation and rearrangement of dislocations and point defects. Recrystallization is the forming of new grains, and is often followed by the coarsening of the recrystallized grain structure. Recovery and recrystallization can take place during and after deformation, the so-called dynamic and static processes, respectively (Figure 1.8) [Hensel and Lehnert, 1973]. Assuming that the driving force for

recrystallization (F_R) is the annihilation of dislocations, then it follows that [Hansen et al., 1980].

$$F_R = \frac{\mu b^2 \Delta \rho}{2} \qquad (1\text{-}13)$$

where, μ is the shear modulus$= 7 \times 10^4$ MPa, b the magnitude of the Burgers vector$= 2.5 \times 10^{-10}$ m and $\Delta\rho$ the change in dislocation density associated with the migration of recrystallization front into the deformed region.
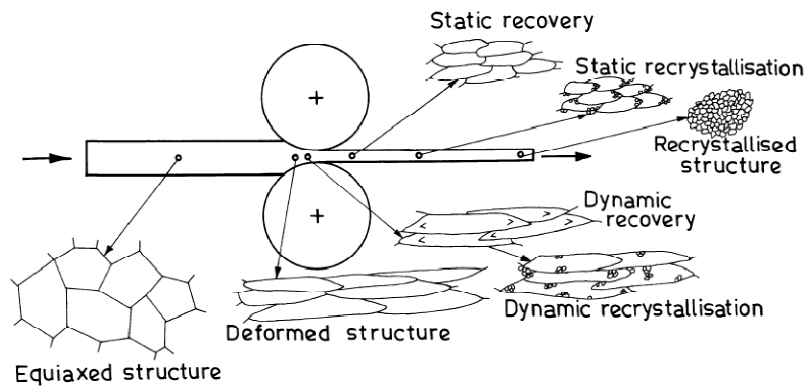

Figure 1.8 Schematic of recovery and recrystallization processes [Hensel and Lehnert, 1973].

Each steel has a temperature T_{nr} which is that above which static recrystallization occurs between the rolling stands, as shown in equation 1-14 [Boratto et al., 1988].

14

$$T_{nr} \, / \, ^\circ C = 887 + 464W_C + 890W_{Ti} + 363W_{Al} - 357W_{Si} + 6445W_{Nb}$$
$$-644\sqrt{W_{Nb}} + 732W_V - 230\sqrt{W_V}$$

(1-14)

where the elements (W) are in wt %.

Equiaxed austenite grains are obtained during deformation above T_{nr} and pancaked grains that temperature. T_{nr} is also affected by microalloying elements as illustrated in figure 1.9 for Fe-0.07C-1.40Mn-0.25Si wt % steel [Cuddy, 1982]. Nb(C,N) is the most potent but the reheating temperature is large enough to dissolve Nb, which then precipitates during rolling as the temperature decreases.
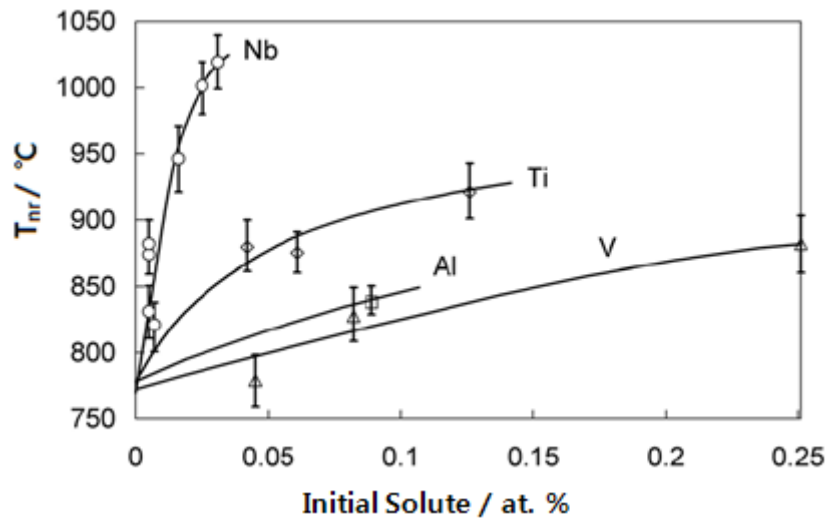

Figure 1.9 Effect of the initial solute content on T_{nr} [Cuddy, 1982].

15

1.2.4 Finishing Mill

The finish-rolling temperature has a large influence on the ferrite grain size and mechanical properties. It is dependent upon the chemical composition of steel and the required mechanical properties.

When $T_{FR} > T_{nr}$, the deformation is known as "recrystallized controlled rolling" [Bleck et al., 1990]. Equiaxed austenite grains are obtained due to recrystallization and grain growth. For $T_{FR} < T_{nr}$, pancaked austenite grains containing deformation bands and deformed annealing twins are produced [DeAdro, 1984]. Ferrite can nucleate not only on the austenite grain boundaries but also on deformation bands and twins [Tanaka, 1984]. Hence, the ferrite grain size will be finer than when deformation is above T_{nr}.

As T_{FR} drops below A_{r3} which is the transformation temperature of the austenite to ferrite during cooling ferrite nucleates on the austenite grain boundaries. If this ferrite and austenite are deformed by finishing rolling, new ferrite grains nucleate on the deformed austenite grain boundaries and also intragranularly on dislocations [Priestner et al., 1976]. The deformed ferrite may then recrystallize into finer ferrite depending upon the temperature. As a result, a structure of deformed ferrite, recrystallized ferrite and pearlite are formed [Tanaka 1981].

If T_{FR} is in the fully ferritic region, the process is called "ferritic rolling" or "warm rolling" [Perry et al., 2000; Tomitz and Kaspar, 2000]. It is used mainly for steels containing < 0.01 wt % carbon and low nitrogen (30ppm) [Hoile, 2000]. Warm rolling is associated with a reduction in the rolling load and hence in energy consumption, less roll wear and reduced runout table water consumption.

1.2.5 Coiling

The coiling temperature can dramatically influence the scale of the microstructure, including ferritie grain size and morphology, interlamellar spacing of pearlite, pearlite lamellar thickness and grain boundary cementite thickness. T_C can be controlled by varying T_{FR} and the cooling rate at the runout table. A low T_C lies in the range of 550-650 ℃ and is associated with a high cooling rate, leading to a greater supercooling and resulting in fine ferrite [Zrnik, 2003]. Pancaked austenite leads to even greater refinement upon coiling [DeAdro, 1984]. A high coiling temperature is above A_{r1} which is the temperature that corresponds to the onset of cementite during the cooling. For this case, both ferrite and austenite coexist in the coil after coiling. Coarsened cementite clusters appear on the grain boundaries after austenite transformation to ferrite. High T_C is associated with low cooling rates, resulting in a coarse microstructure.

1.3 Neural network

Materials science and metallurgy has been developed over many years but there are phenomena which are too complex to fully understand because of their multivariate nature. For example, the mechanical properties of hot-rolled steels are affected by many process-variables. This is a reason why general methods for the prediction of final mechanical properties are lacking. Nevertheless there have been many attempts to model mechanical properties using linear equations [Pickering, 1978]

$$\sigma_Y, \mathrm{MPa} = 53.9 + 32.3W_{Mn} + 83.2W_{Si} + 354.2W_{Nf}^{0.5} + 17.4d_\alpha^{-0.5} \qquad (1\text{-}15)$$

$$\sigma_U, \mathrm{MPa} = 294.1 + 27.7W_{Mn} + 83.2W_{Si}$$
$$+3.85(\%pearlite) + 7.7d_\alpha^{-0.5} \qquad (1\text{-}16)$$

where σ_Y is the predicted yield strength in MPa, W_{Mn}, W_{Si} and W_{Nf} are the contents of manganese, silicon and free nitrogen in weight percent, and d_α is the ferrite grain size in millimeters.

However, such empirical, linear equations have problems because there is no modeling uncertainty, as will be discussed later, and the variables are independently considered. Neural networks are better suited to those problems not only in the study of mechanical properties but wherever the complexity of the problem is inevitable.

A neural network is a paramerterized nonlinear model and its flexibility makes it able to discover more complex relationships in data than traditional statistical models. Bayesian probability theory provides a unifying framework for data modeling which offers several benefits. First, the overfitting problem can be solved by using Bayesian method to control model complexity. Second, probabilistic modeling handles uncertainty in a natural manner [MacKay, 1995].

1.3.1 Nonlinear regression

A neural network uses a flexible non-linear function, for example:

$$y = \sum_i w_i h_i + \theta \qquad (1\text{-}17)$$

$$h_i = \tanh\left(\sum_j w_{ij} x_j + \theta_j\right) \qquad (1\text{-}18)$$

where x_j are the j th input variables on which the output y depends, w_i are the weights, and θ_j are the biases which are similar to the constants of linear function. Neural networks can vary their flexibility by varying the weights (Figure 1.10a), combining several of the hyperbolic tangents or changing the number of hidden units i (Figure 1.10b) and controlling the number of inputs (Figure 1.10c), making the neural network capture arbitrary relationship [Bhadeshia, 2006; McKay, 1995]. Figure 1.11 shows a schematic neural network model which has three inputs, two hidden units and one hidden layer. Since the weights and the constants were chosen at random, the value of the output will not match with experimental data at first attempt. The weights are thus systematically changed until a best-fit description of the output is obtained as a function of the inputs [Bhadeshia and Sourmail, 2003]. A network as defined in equation 1-17 and 1-18 is trained using a data set $D = \{x^{(m)}, t^{(m)}\}$ by adjusting w so as to minimize an objective function (Equation 1-19) as follows [MacKay, 1992]:

$$M(w) = \alpha E_D + \beta E_w \qquad (1\text{-}19)$$

$$E_D(w) = \frac{1}{2} \sum_m \sum_i (t_i^{(m)} - y_i(x^{(m)}; w))^2 \qquad (1\text{-}20)$$

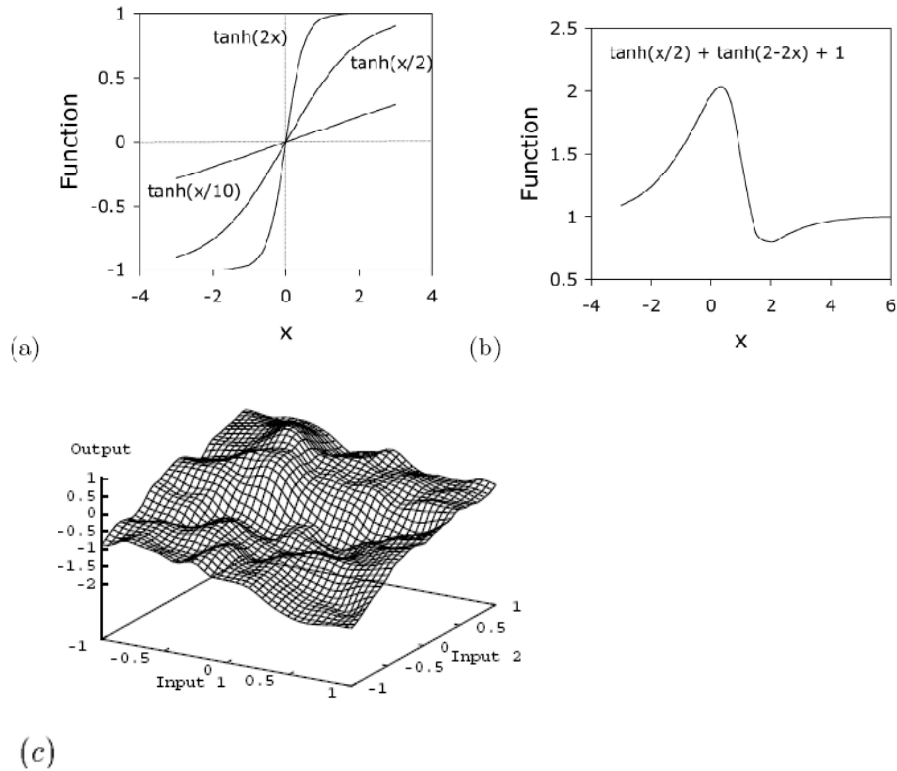$$E_w = \frac{1}{2} \sum_i w_i^2 \qquad (1\text{-}21)$$

Figure 1.10 (a) Three different hyperbolic tangent functions by varying the weights of one variable. (b) A combination of two hyperbolic tangents of one variable to produce a more complex model. (c) A typical function produced by two inputs network [Bhadeshia, 2006; McKay, 1995].

The error function (Equation 1-20) is a sum of terms, one for each input/output pair *{x, t}*, measuring how close the predicted output *y(x; w)* is to measured output *t*. The regularization function (Equation. 1-21) favors small values of *w* and thus encourages the model to find simpler solutions with less tendency to overfitting. The control parameter α and β determine the complexity of the model.

$$\sigma_w^2 = \frac{1}{\alpha} \qquad (1\text{-}22)$$

$$\sigma_v^2 = \frac{1}{\beta} \qquad\qquad (1\text{-}23)$$

where σ_w is a weight variance and σ_v is a perceived level of noise. The weights of an input with a large value of α have more of a tendency to decay to zero, so such an input is not significant in the regression. This process is known as training and the network and the details are described by MacKay [1992; 1993; 1995; 1997].
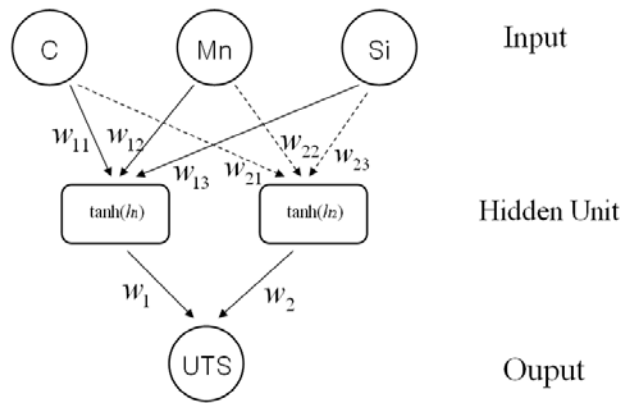

Figure 1.11 Schematic of neural network for three inputs (C, Mn and Si) and two hidden units.

1.3.2 Optimization of Model Complexity

The original data are randomly divided into two sets, training data set and testing data set. And the data are normalized in the range of ± 0.5 according to

$$x_N = \frac{x - x_{min}}{x_{max} - x_{min}} - 0.5 \qquad (1\text{-}24)$$

where x is original value, x_{max}, x_{min} are the maximum and minimum value in the database, and x_N is the normalized value. This process is not an essential for the neural network but gives a convenient way to compare the results of prediction for different inputs. The model is produced by using only the training dataset and then is checked using test data set to avoid the overfitting problem when the function is over complex because of too many hidden units. Overfitting phenomenon is described in figure 1.12, which shows an optimal complexity by evaluating a test error. When the complexity of model increases, the model makes an over precise relationship between the input and output (Figure 1.12a to c), but the test error evaluated from unseen data will increase after a certain point (figure 1.12 d) [MacKay, 1995].
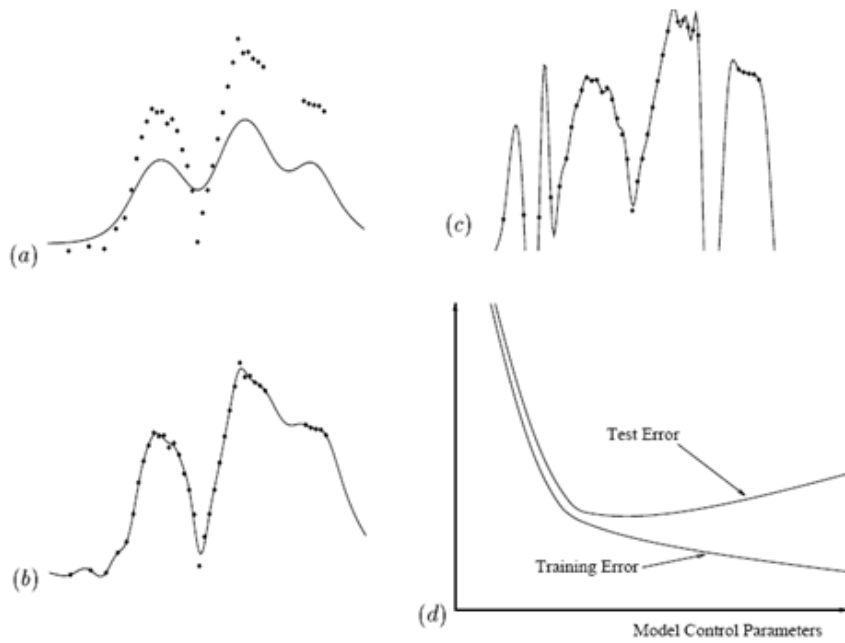
Figure 1.12 Optimization of model complexity. As the complexity increase (from a to c), the interpolant is able to fit the training data well, but beyond a certain point the generalization ability (test error) of the model deteriorates (d) [MacKay, 1995].

Each model which has different numbers of hidden unit or initial seed, is usually ranked by minimum test error. However, typically the sum of test errors with several good models can be less than that of the best single model (Figure 1.13). Therefore the committee of models is used for a final prediction. The following formula gives the error bars for predictions of a committee consisting of N equally weighted members.

Committee prediction $\quad \bar{y} = \frac{1}{N}\Sigma_i\, y^{(i)}$ $\qquad\qquad$ (1-25)

Variance $\qquad \sigma^2 = \frac{1}{N}\Sigma_i\, \sigma_y^{(i)^2} + \frac{1}{N}\Sigma_i(y^{(i)} - \bar{y})^2$ $\qquad$ (1-26)
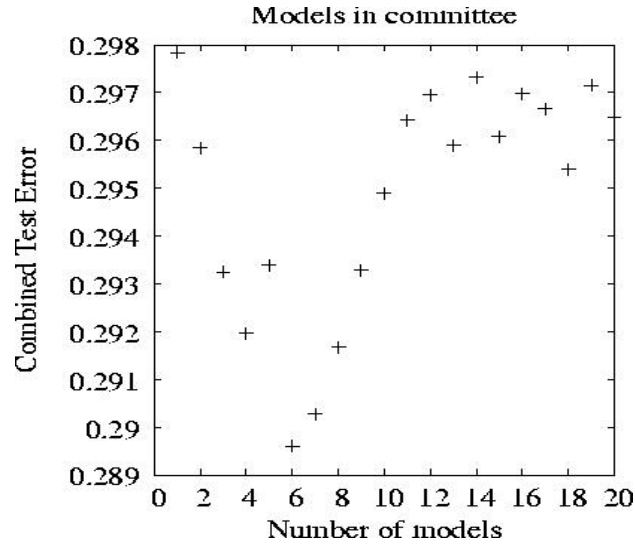
23

Figure 1.13 Combined test error depends on the number of models. The test error of committee, sum of six models, is less than the one for the best single model.

Often, it is a more appropriate to evaluate the performance of a model by using the log predictive error (LPE). This error penalises large test errors, but compensates if the prediction has large error bars [MacKay, 1995].

$$LPE = \sum_i [\frac{\frac{1}{2}(t_i - y_i)^2}{\sigma_y^{i^2}} + \log{(2\pi\sigma_y^i)^{\frac{1}{2}}}] \qquad (1\text{-}27)$$

1.3.3 Noise and Uncertainty

Noise is an error associated with the influence of uncontrolled variables. Noise can be expressed by the variance between predicted and measured values:

$$\sigma_v = \sqrt{\sum_{j=1}^n \frac{(t_j - y_j)^2}{n^2}} \qquad (1\text{-}28)$$

24

Figure 1.14a shows this noise when the straight line is fitted with a standard error of ± 2 in the estimation of the output y [Bhadeshia, 2006]. On the other hand figure 1.14b shows one example of modeling uncertainty. Two functions are fitted to the given training or experimental data. One is linear $y=2x$ and the other is non-linear $y = -\frac{x^3}{44} + \frac{3x^2}{11} + \frac{34x}{11}$. These two functions give different predictions, and the difference can be used as a measure of the uncertainty, for the input 8 and 10 where training data do not exist.
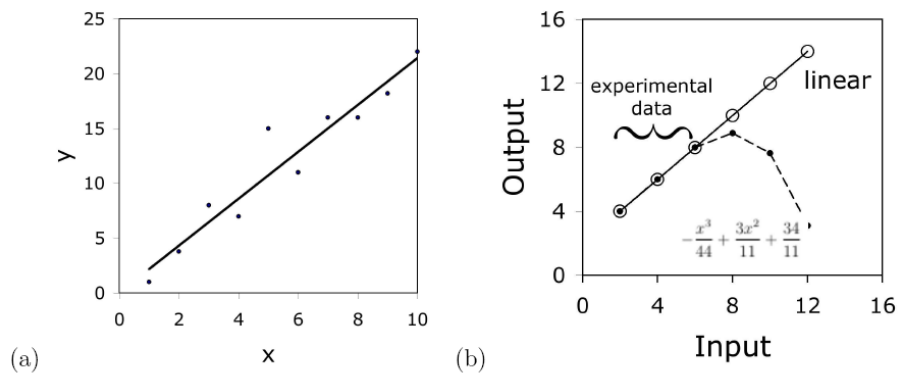

Figure 1.14 (a) Noise (b) Uncertainty [Bhadeshia, 2006].

MacKay has developed a useful treatment of neural networks in a Bayesian framework, which allows the calculation of error bars representing the uncertainty in the fitting parameters [MacKay, 1992]. Instead of calculating a unique set of weights, a probability distribution of sets of weights is used to define the fitting uncertainty. The error bars become large when data are sparse or noise. However, large uncertainty always identifies a need for a research and leaves open the possibilities [Bhadeshia, 2006].

II Details of Modeling

2.1 Input and Output

All of the data used in this work are from the Sheet Products and Process Research group of the steel company, POSCO. The specimens on which the mechanical properties are determined come from the tails of hot-rolled coils. The specimens are cut just after the coils reach ambient temperature during cooling in air.

The chemical composition of the steels studied includes carbon, manganese, silicon, phosphorus, sulphur, chromium, nickel, molybdenum, titanium, niobium, vanadium, aluminum, nitrogen, boron, copper, tin and calcium. The finish-rolling temperature (T_{FR}), coiling temperature (T_C), coil thickness (C_t), reheating time (t_R), reheating temperature (T_R) and total reduction ratio (ε_r, equation 2-1) are considered as the thermo-mechanical variables of the hot rolling process:

$$\varepsilon_r = \frac{L_{F0} - L_{F7}}{L_{F0}} \tag{2-1}$$

where L_{F0} and L_{F7} are the thicknesses of plate before and after the finishing rolling respectively.

Two sets of data are used for the modeling in this work, as described in tables 2.1 and 2.2, where the range, means and standard deviations of the variables are listed. The chemical composition and thermo-mechanical variables are the input variables, and the ultimate tensile strength (σ_U), yield strength (σ_Y) or percent elongation (ϵ) are the outputs. The datasets show almost identical mean values for each variable. However, the second set of data contains a few cases which are solute-rich. For example, there are 59 data for which the Nb concentrations are higher than 0.01 wt %, which form a small proportion of

26

the total set. They nevertheless are important in reducing the uncertainties and hence in raising the predictive power of the models.

In this work, ten separate committee models were produced to enable comparisons between the different approaches, table 2.3.

	Minimum	Maximum	Mean	St. Dev.
C / wt %	0.0204	0.8684	0.1009	0.0833
Mn / wt %	0.167	1.41	0.471	0.2177
Si / wt %	0	0.217	0.0146	0.0262
P / wt %	0.004	0.022	0.0129	0.0027
S / wt %	0.002	0.015	0.007	0.0023
Cr / wt %	0	0.16	0.0189	0.0137
Ni / wt %	0	0.06	0.0132	0.006
Mo / wt %	0	0.02	0.0008	0.0028
Ti / wt %	0	0.004	0.0006	0.0009
Nb / wt %	0	0.004	0.0002	0.0004
V / wt %	0	0.003	0.0011	0.001
Al / wt %	0	0.064	0.0323	0.0105
N / ppm	0	87	33.8483	13.4774
B / ppm	0	2	0.2888	0.473
Cu / wt.%	0	0.03	0.0075	0.0061
T_{FR} / ℃	808	925	868.876	14.089
T_C / ℃	478	714	618.7996	29.5304
σ_U / MPa	317	1039	411.4461	69.6126
σ_Y / MPa	193	627	292.4937	43.047
ϵ / %	14	50	38.4658	6.3109

Table 2.1: The variables in the first dataset consisting of 3508 experiments.

	Minimum	Maximum	Mean	St. Dev.
C / wt %	0.0012	0.8684	0.1009	0.0842
Mn / wt %	0.045	1.41	0.4763	0.2237
Si / wt %	0	1.954	0.0216	0.0594
P / wt %	0.003	0.11	0.0133	0.0055
S / wt %	0	0.017	0.0069	0.0025
Cr / wt %	0	0.46	0.0203	0.0266
Ni / wt %	0	0.44	0.0152	0.0239
Mo / wt %	0	0.2	0.0009	0.0044
Ti / wt %	0	0.058	0.0008	0.0035
Nb / wt %	0	0.041	0.0005	0.0026
V / wt %	0	0.041	0.0014	0.0018
Al / wt %	0	0.288	0.0319	0.0123
N / wt %	0	0.0087	0.0034	0.0014
B / wt %	0	0.0002	0.000026	0.000046
Cu / wt %	0	0.54	0.0098	0.0283
Sn / wt %	0	0.008	0.0019	0.0014
Ca / wt %	0	0.0032	0.0001	0.0004
T_{FR} / ℃	700	930	867.3663	14.6396
T_C / ℃	449	695	600.0074	26.9377
C_t / mm	1.4	12.7	4.76	2.56
t_R / min	116	903	205.7459	82.9132
T_R / ℃	1128	1247	1145.671	12.1482
ε_r	0.7214	0.9696	0.9039	0.0476
σ_U / MPa	292	1039	413.6963	71.9043
σ_Y / MPa	150	676	296.8	47.0699
ϵ / %	13	53	38.3439	6.3722

Table 2.2: Variables in the second dataset consisting of 3385 experiments. The maximum values of the solute concentration are higher than those of the first dataset except for C, Mn, Si, N and B.

Model Name	Data	Output	Inputs
M_σ_UF17	First Dataset	σ_U	C, Mn, Si, P, S, Cr, Ni, Mo, Ti, Nb, V, Al, N, B, Cu, T_{FR}, T_C
M_σ_YF17		σ_Y	
M_ϵF17		ϵ	
M_σ_US19	Second Dataset	σ_U	C, Mn, Si, P, S, Cr, Ni, Mo, Ti, Nb, V, Al, N, B, Cu, Sn, Ca, T_{FR}, T_C
M_σ_YS19		σ_Y	
M_f{ϵ}S19		$f\{\epsilon\}$	
M_σ_US23		σ_U	C, Mn, Si, P, S, Cr, Ni, Mo, Ti, Nb, V, Al, N, B, Cu, Sn, Ca, T_{FR}, T_C, C_t, t_R, T_R, ε_r
M_σ_YS23		σ_Y	
M_ϵS23		ϵ	
M_f{ϵ}S23		$f\{\epsilon\}$	

Table 2.3: Inputs, output and dataset of the each committee model.

The outputs of models M_f{ε}S19 and M_f{ε}S23 are $f\{\epsilon\}$ (logarithmic elongation) based on equation 2-1. The elongation of the steel cannot be negative, and yet empirical functions are capable of making such predictions. To avoid this, a natural logarithm functional is defined which cannot give a negative values for x on removing the logarithm [Yescas *et al*., 2001].

$$f\{\epsilon\} = \ln\left\{-\ln\left(1 - \frac{(\epsilon_{max} - \epsilon)}{(\epsilon_{max} - \epsilon_{min})}\right)\right\} \qquad (2\text{-}2)$$

where ϵ_{max} and ϵ_{min} represent maximum and minimum values set by the user in order to confine the uncertainties and predictions within the range ϵ_{max}-ϵ_{min}.

Committee model M_ϵS23, which directly estimates elongation, is not mathematically limited in any way unlike models M_f{ϵ}S19 and M_f{ϵ}S23

in which the predictions are bounded. In this work, ϵ_{max} is set to 80 percent elongation and ϵ_{min} 8, but these values don't have a special meaning.

Figures 2.1 to 2.23 show visual impressions of the spread in the values of particular input variables as a function of σ_U in the second dataset. In the present work, a Bayesian framework based neural network was used [MacKay, 1992], which makes it possible to calculate of the uncertainty of modeling. The latter varies with the position in the input space for which a calculation is done, and hence defines the range of useful applicability of the model. The concentrations of most solutes are minute, but sometimes the alloys are richly alloyed for special purposes. Figure 2.24 shows the distribution of carbon versus for σ_Y, and figure 2.25 the carbon versus ϵ, in both cases for the second dataset. The first set of data also show similar distributions with respect to σ_U, σ_Y and ϵ.
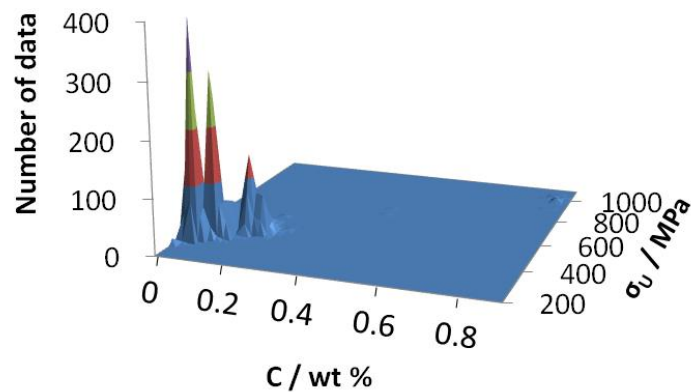
Figure 2.1 Distribution of carbon versus σ_U in the second dataset
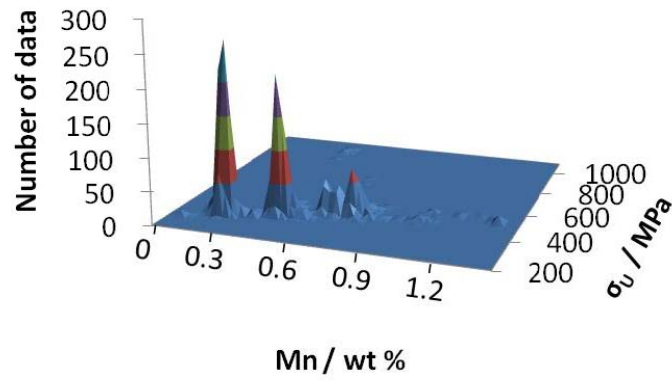
Figure 2.2 Distribution of manganese versus σ_U in the second dataset.
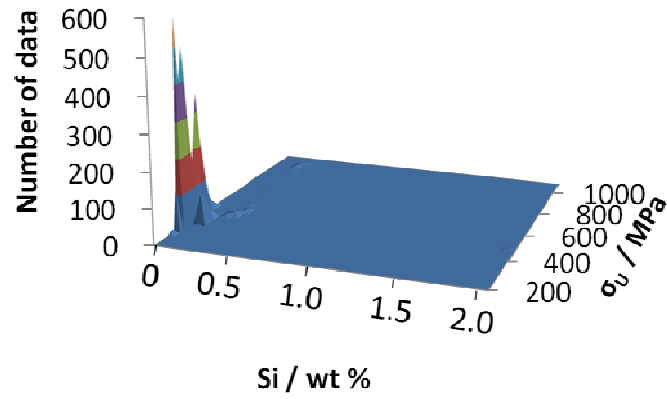
Figure 2.3 Distribution of silicon versus σ_U in the second dataset.
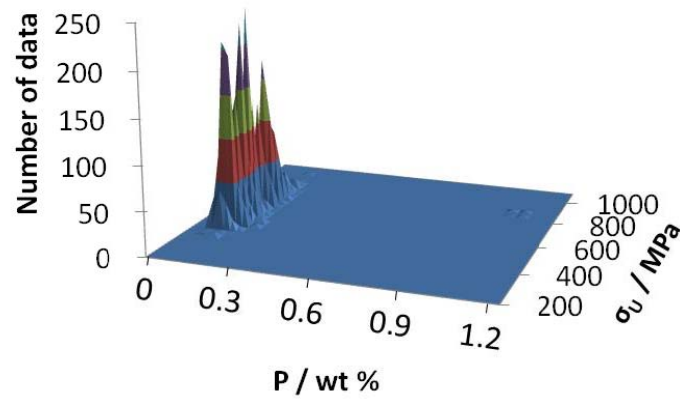
Figure 2.4 Distribution of phosphorus versus σ_U in the second dataset.
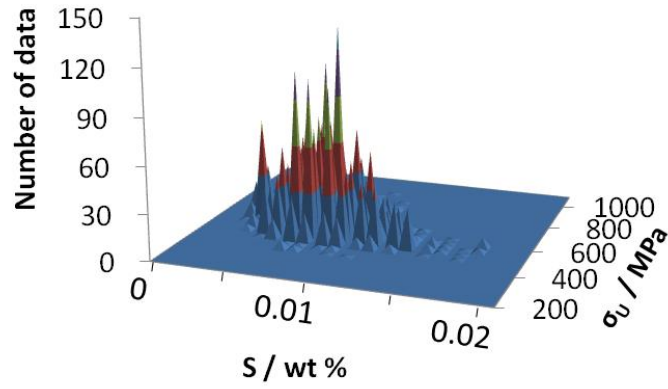
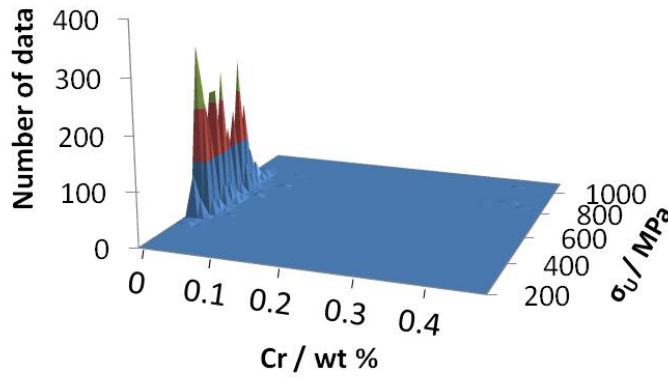Figure 2.5 Distribution of sulfur versus σ_U in the second dataset.

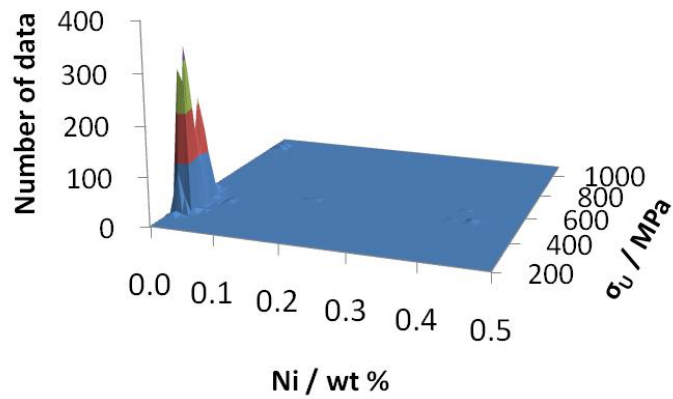Figure 2.6 Distribution of chromium versus σ_U in the second dataset.

Figure 2.7 Distribution of nickel versus σ_U in the second dataset.
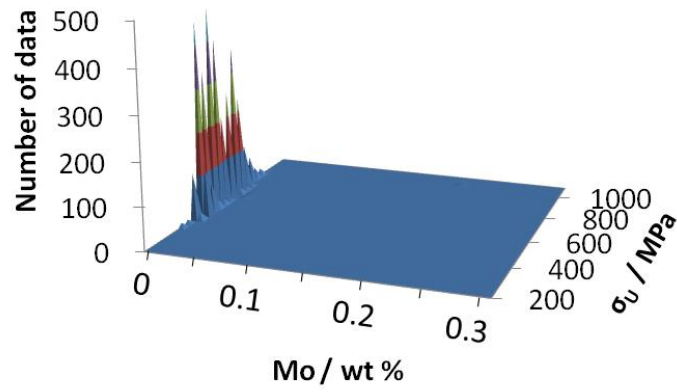
Figure 2.8 Distribution of molybdenum versus σ_U in the second dataset.
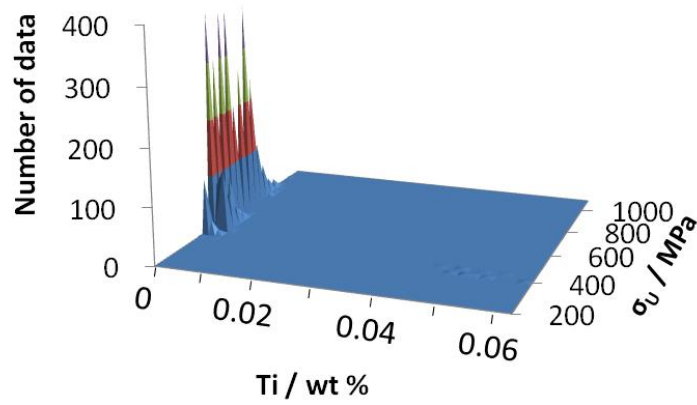
Figure 2.9 Distribution of titanium versus σ_U in the second dataset.
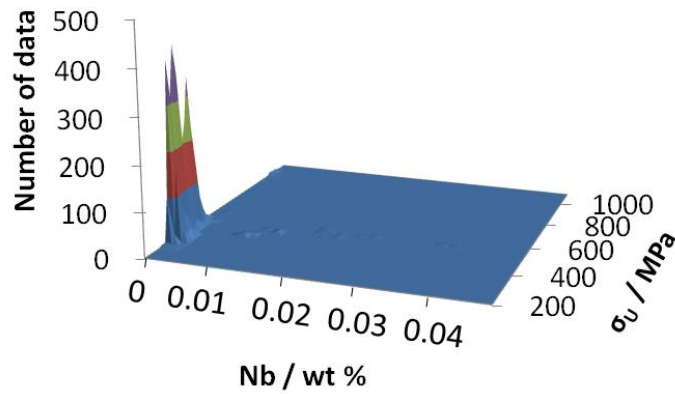
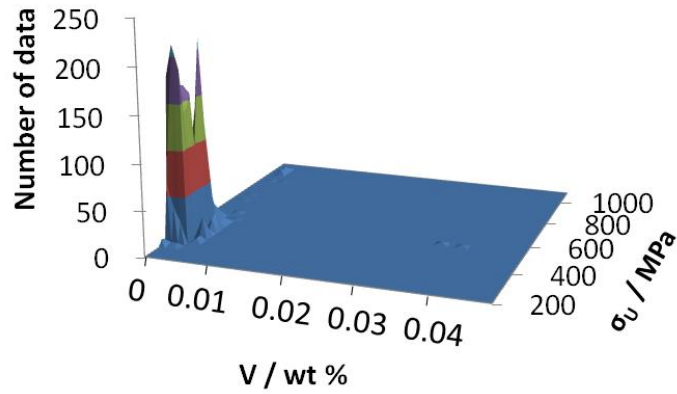Figure 2.10 Distribution of niobium versus σ_U in the second dataset.

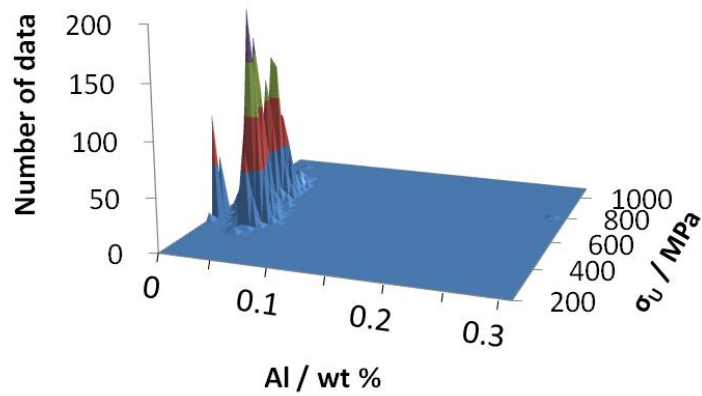Figure 2.11 Distribution of vanadium versus σ_U in the second dataset.

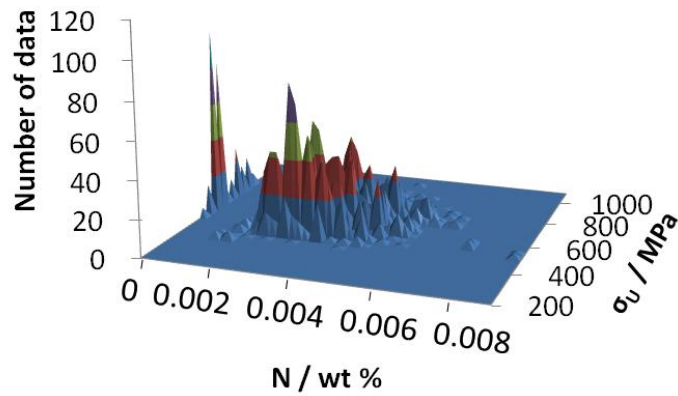Figure 2.12 Distribution of aluminum versus σ_U in the second dataset.

Figure 2.13 Distribution of nitrogen versus σ_U in the second dataset.
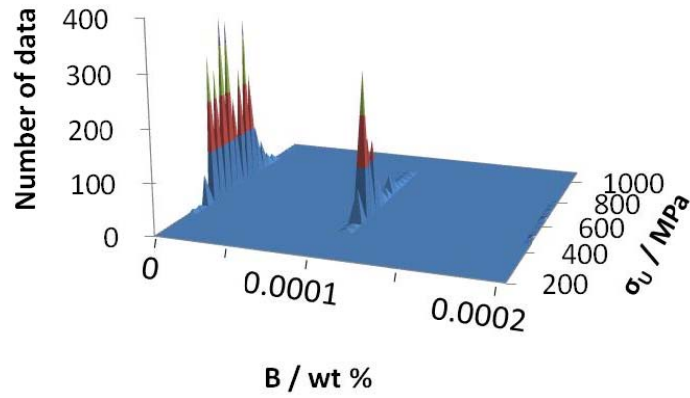
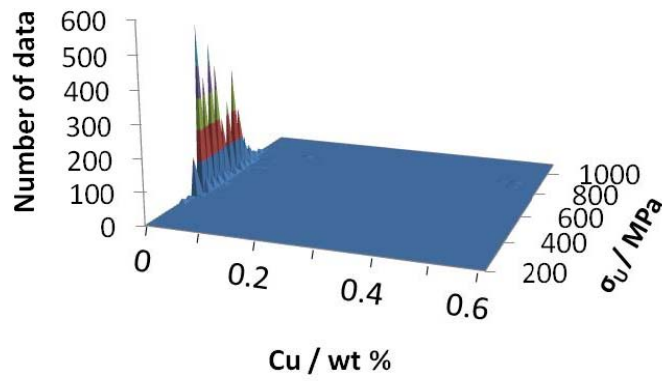Figure 2.14 Distribution of boron versus σ_U in the second dataset.

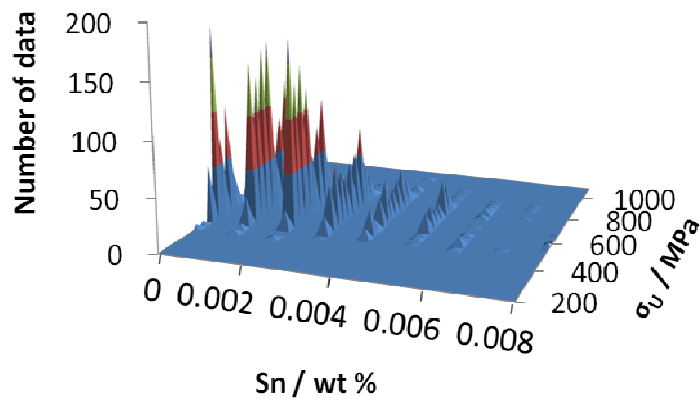Figure 2.15 Distribution of copper versus σ_U in the second dataset.

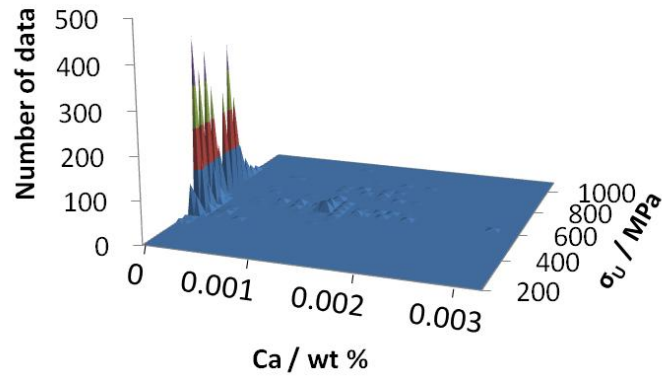Figure 2.16 Distribution of tin versus σ_U in the second dataset.

35

Figure 2.17 Distribution of calcium versus σ_U in the second dataset.
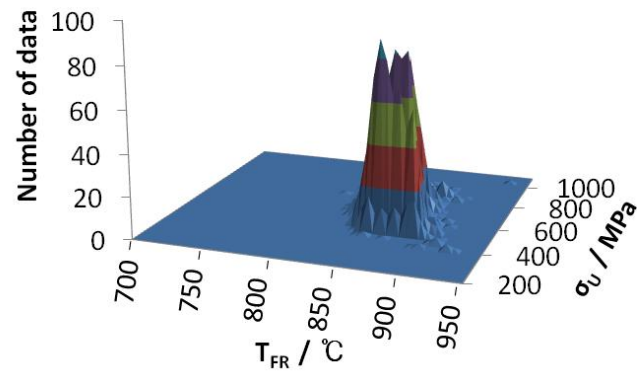
Figure 2.18 Distribution of finish-rolling temperature versus σ_U in the second dataset.
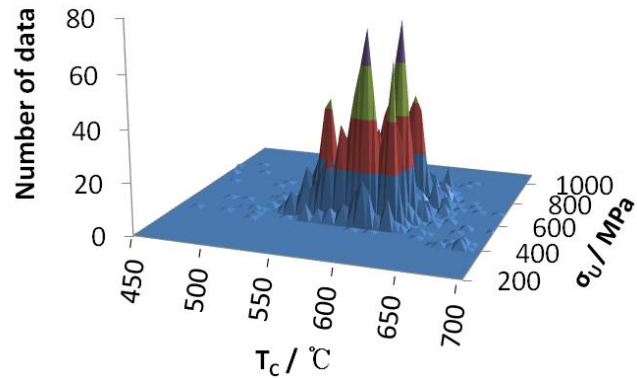
Figure 2.19 Distribution of coiling temperature versus σ_U in the second dataset.
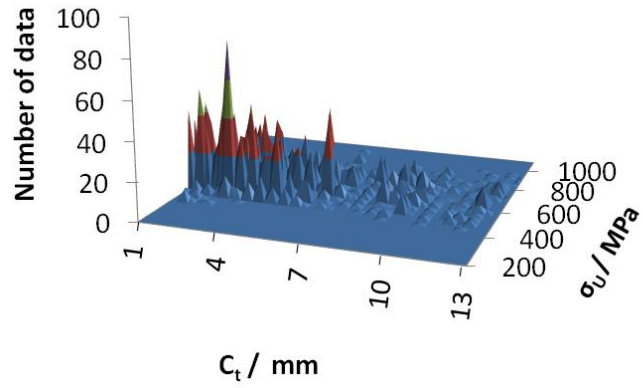
Figure 2.20 Distribution of coil thickness versus σ_U in the second dataset.
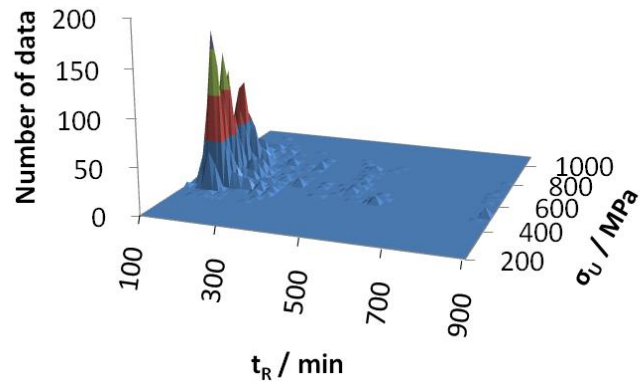
Figure 2.21 Distribution of reheating time versus σ_U in the second dataset.

Figure 2.22 Distribution of reheating temperature versus σ_U in the second dataset.

Figure 2.23 Distribution of total reduction ratio versus σ_U in the second dataset.

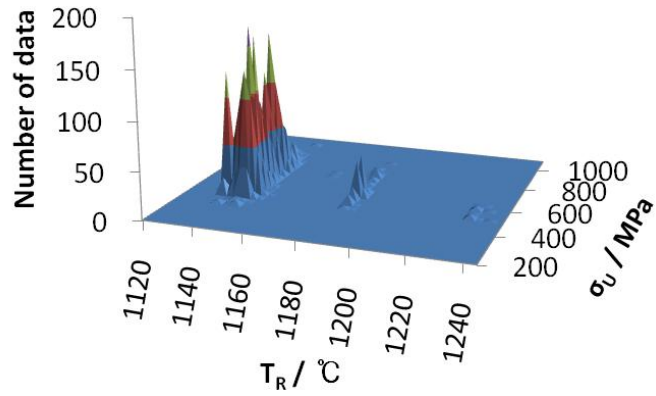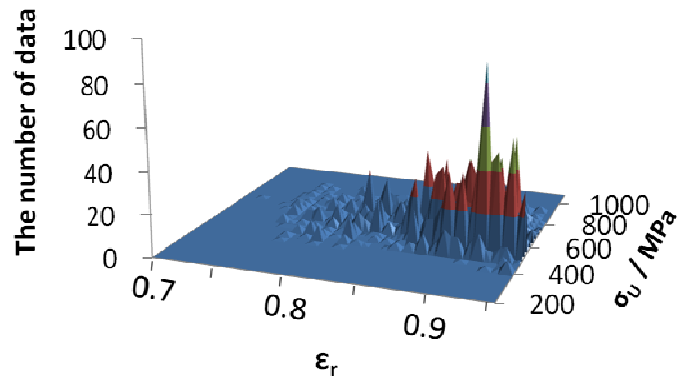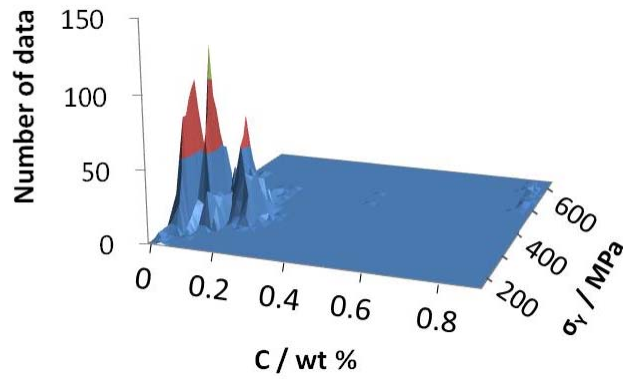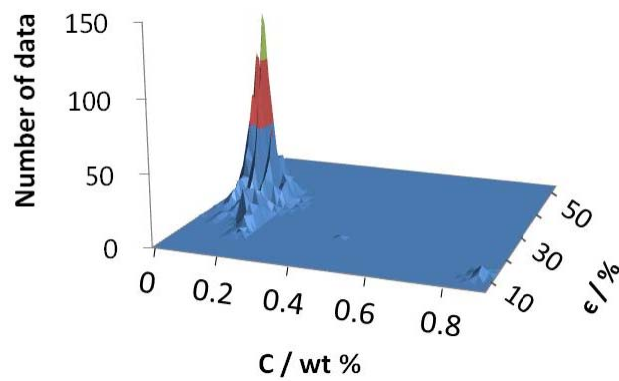Figure 2.24 Distribution of carbon versus σ_Y in the second dataset.

Figure 2.25 Distribution of carbon versus ϵ in the second dataset.

38

2.2 Training and Testing

The data were randomized and then partitioned equally into test and training sets. The latter was used to create a large variety of neural networks models whereas the test data set was used to see how the trained models generalized on unseen experiments. One hundred models were trained to produce the committee model using the training dataset. Each model has a different number of hidden units and random seeds used to initiate the values of weights. Figure 2.26 gives the training and test results of 100 models for the committee model M_σ_UF17. The perceived level of noise σ_v decreases as the hidden units increase, which means that more a complex model has the lower σ_v (Figure 2.26a). However, the log predictive error (LPE) reaches a maximum at 15 hidden units (Figure 2.26b). The number of hidden units is set by examining the performance of the model on unseen test data, and the test error reaches a minimum at 11 hidden units (Figure 2.26c). Good models are ranked by the test error in order to discover the optimum committee model. One containing eleven of the best models was found to be an optimum with the smallest test error, as shown in figure 2.26 (d). The selected committee then is retrained on the entire dataset without changing the complexity of its member models. Figure 2.27 shows a plot of measured versus predicted output using the committee model M_σ_UF17 on the whole dataset. There are a few outliers and very small error bars which represent the combined effect of modeling uncertainty σ_w and the perceived level of noise σ_v.
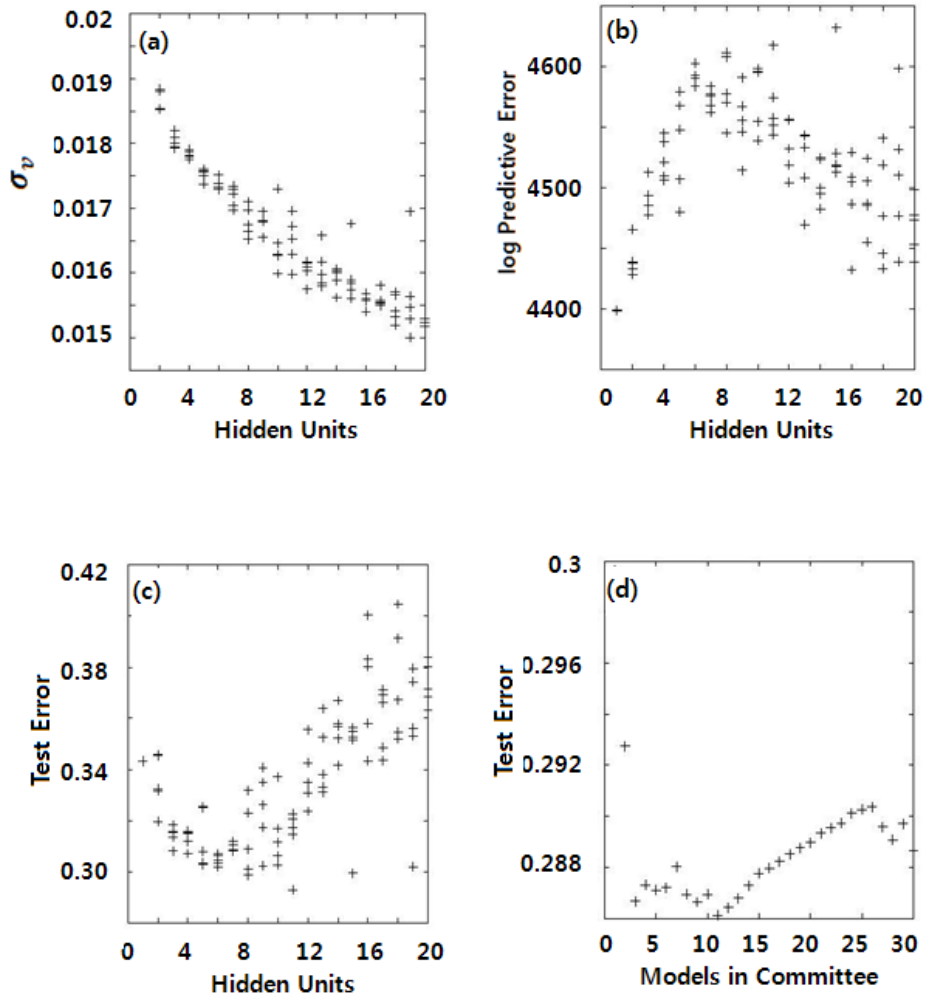
Figure 2.26 Characteristics of the committee model M_σ$_U$F17. (a) Perceived level of noise σ_v versus hidden unit (b) log predictive error versus hidden unit (c) test error versus hidden unit (d) test error versus number of models in the committee.
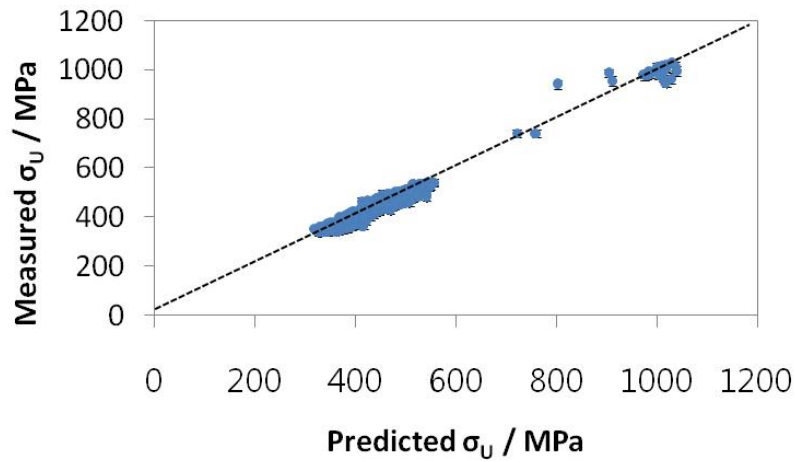
Figure 2.27 Measured σ_U versus predicted σ_U of the committee model M_σ_UF17.

All committee models from 1 to 10 are trained and tested in the same manner, and their training and test results are described in table 2.4. The noise, LPE, test error and the number of hidden units are values of the best model of each committee. The elongation models show relatively high noise. However, the noise and test errors of the models can be decreased by adding proper input variables (figure 2.28).
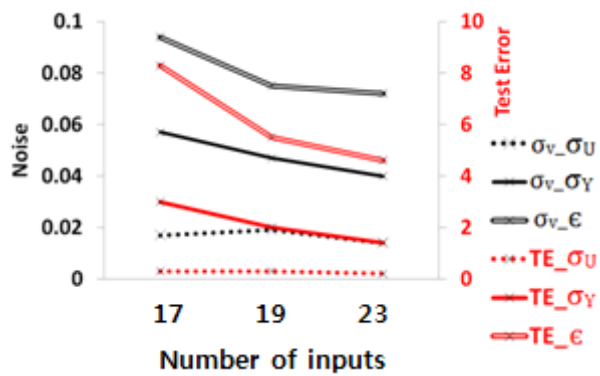
Figure 2.28 Noise and test errors for all committees.

Model	Output	Noise σ_v	LPE	Test Error	Number of hidden units	Number of models in committee
M_σ_UF17	σ_U	0.017	4550	0.3	11	11
M_σ_YF17	σ_Y	0.057	2490	3.0	2	5
M_ϵF17	ϵ	0.094	1570	8.3	8	3
M_σ_US19	σ_U	0.019	4334	0.3	3	6
M_σ_YS19	σ_Y	0.047	2740	2.0	5	7
M_f{ϵ}S19	$f\{\epsilon\}$	0.072	2058	4.6	6	5
M_σ_US23	σ_U	0.014	4690	0.2	14	3
M_σ_YS23	σ_Y	0.040	3027	1.4	5	4
M_ϵS23	ϵ	0.075	1884	5.5	7	4
M_f{ϵ}S23	$f\{\epsilon\}$	0.062	2238	3.6	5	10

Table 2.4: Training and test results of the committee models.

Figures 2.28 to 30 indicate the significances σ_w of input variables, as perceived by the first three models in the respective committee. The significance indicates the level of contribution to the output, rather like a partial correlation coefficient in linear regression analysis. C, Mn and Si give relatively large contributions to the tensile strength, and microalloying elements (Ti, Nb, V) also show similar significances even though their concentrations vary in the narrow ranges as compared with the former chemical elements (Figure 2.28). In the cases of yield strength model and elongation model, C, Mn, Si, Nb, C_t and ϵ_r contribute more to the outputs (figure 2.29, 30).
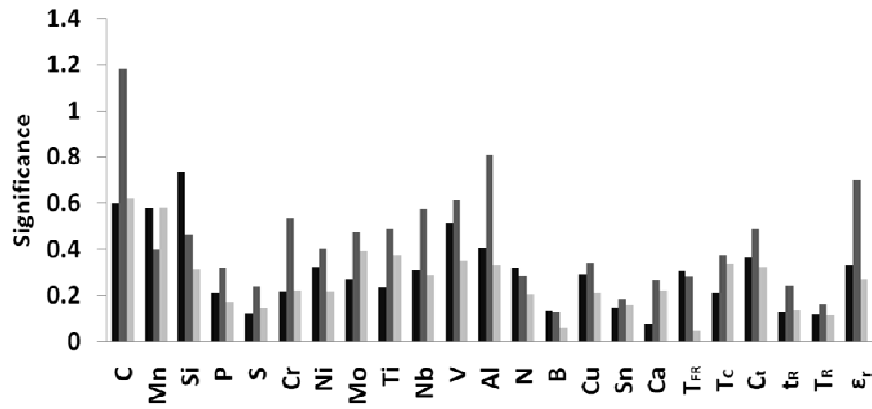
Figure 2.28 Significance σ_w of each variable of the model M_σ_US23. C, Mn and Si contribute to the σ_U more than other variables, however each variable shows a moderate significance.
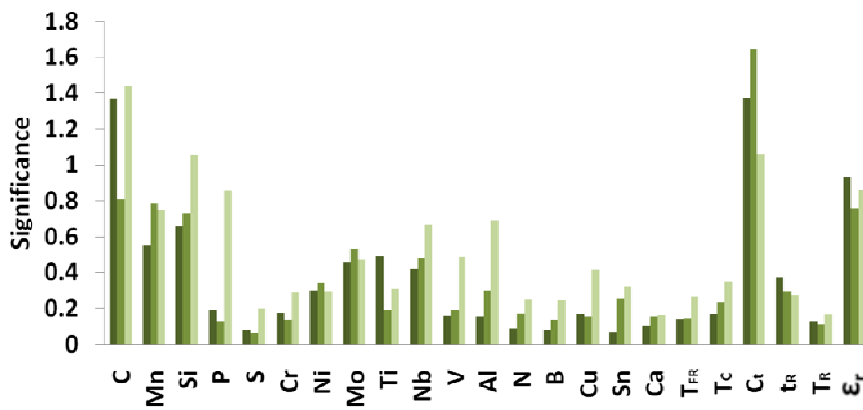
Figure 2.29 Significance σ_w of each variable for the σ_Y of model M_σ_YS23. C_t and ε_r are remarkable among the thermo-mechanical variables

43
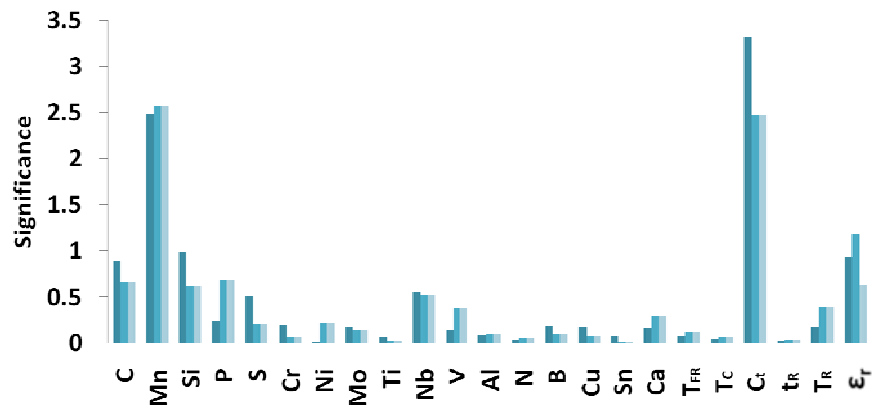
Figure 2.30 Significance σ_w of each variable of the model M_ϵS23. Mn and C_t give the largest contribution to the ϵ.

III   Application of model

The optimized committee consisting of ten models was used to study the effects of individual variables on the tensile properties σ_U, σ_Y and ϵ to find out whether the results are compatible with known metallurgical principles and other published trends not incorporated in the models. The compositions used for the predictions are listed in table 3.1. Alloys A and B were set at the mean values given in table 2.1 and 2.2 respectively. The compositions C, D and E were obtained from the literature [Hashimoto, 2003; Mesplont, 2006; Zrnik, 2003]. When the full information was not reported with respect to the rolling schedule, it was assumed that the parameters corresponded to the mean values used here. When studying the effect of a particular variable, the remaining inputs were as listed in table 3.1. All the error bars represent the combined effect of the uncertainty ($\pm 1\,\sigma$) and noise of the committee model.

3.1 General Solutes

C, Mn and Si contribute to the outputs as shown in figures 2.28 to 2.30. Figure 3.1 shows the results with the predicted σ_U, σ_Y and ϵ versus the C concentration for alloy A. The σ_U and σ_Y increase, and ϵ decreases as C increases, although the uncertainty becomes larger. These are expected trends, which indicate that the models exhibit reasonable behavior. In steels of the type considered here, an increase in the carbon concentration should lead to a greater fraction of pearlite which a composite of Fe_3C and ferrite, is harder than ferrite or its own. It is interesting that the ultimate tensile strength is more sensitive to carbon than the yield strength. This is consistent with experimental observations [Singh et al., 1998; Pickering, 1978; Shimizu et al., 1986]. When a ferrite-pearlite ($\alpha + P$) mixed microstructure is strained, plastic flow begins in the softer allotriomorphic ferrite, while the pearlite is

45

elastically deformed [Bhadeshia and Edmonds, 1980]. As a result, the yield strength is insensitive to the fraction of pearlite, and hence to the amount of carbon. However, both constituents $(\alpha + P)$ participate in plasticity at large ϵ, making the ultimate tensile strength more sensitive to the pearlite fraction or carbon concentration.

	A	B	C	D	E
C / wt %	0.1009	0.1009	0.046	0.058	0.1
Mn / wt %	0.471	0.4763	1.19	0.52	0.91
Si / wt %	0.0146	0.0216	0.03	0	0.01
P / wt %	0.0129	0.0133	0.015	0	0.011
S / wt %	0.007	0.0069	0.002	0	0.008
Cr / wt %	0.0189	0.0203	0	0	0
Ni / wt %	0.0132	0.0152	0	0	0
Mo / wt %	0.0008	0.0009	0	0	0
Ti / wt %	0.0006	0.0008	0	0.057	0.04
Nb / wt %	0.0002	0.0005	0.023	0.054	0.03
V / wt %	0.0011	0.0014	0	0	0
Al / wt %	0.0323	0.0319	0.038	0.052	0.04
N / wt %	0.0033	0.0034	0.0067	0.0088	0.007
B / wt %	0.000028	0.000026	0	0	0
Cu / wt %	0.0075	0.0098	0	0	0.029
Sn / wt %	-	0	0	0	0
Ca / wt %	-	0	0	0	0
T_{FR} / ℃	867	867	850	880	860
T_{C} / ℃	618	600	450	600	520
C_{t} / $\times 10^{-2}$ mm	-	476	400	400	476
t_{R} / min	-	205	45	60	205
T_{R} / ℃	-	1145.671	1100	1250	1150
ε_{r}	-	0.9039	0.88	0.87	0.9

Table 3.1: Compositions of alloys used to study the effects of individual variables on the tensile properties.

Manganese not only has a strong effect on the stability of the austenite, but also provides solid solution strengthening. Figure 3.2 shows the effects of Mn for alloy A. The Pickering equations reproduced in equations 1-5 and 1-6 attribute 32 and 27 MPa solid solution strengthening increment in σ_Y and σ_U respectively, due to a 1 wt % increase in Mn level. On the other hand, the models here show somewhat larger strength increments (85 and 90 MPa respectively) than the Pickering equations. This is reasonable because manganese has an effect beyond just solid-solution strengthening; the plots in figure 3.2 show the influence of all factors rather than just solution strengthening. Because Mn depresses the transformation temperature, it also refines the microstructure (finer ferrite grain size), so it is reasonable that the strength increments calculated are larger than expected from Pickering's analysis. The abrupt drop in elongation at about 1 wt % Mn is strange since similar effects are not seen in the σ_Y and σ_U curves. It is possible that this is associated with the onset of microstructural banding [Sakir, 1991], which is known to become more prominent as the Mn concentration is increased.
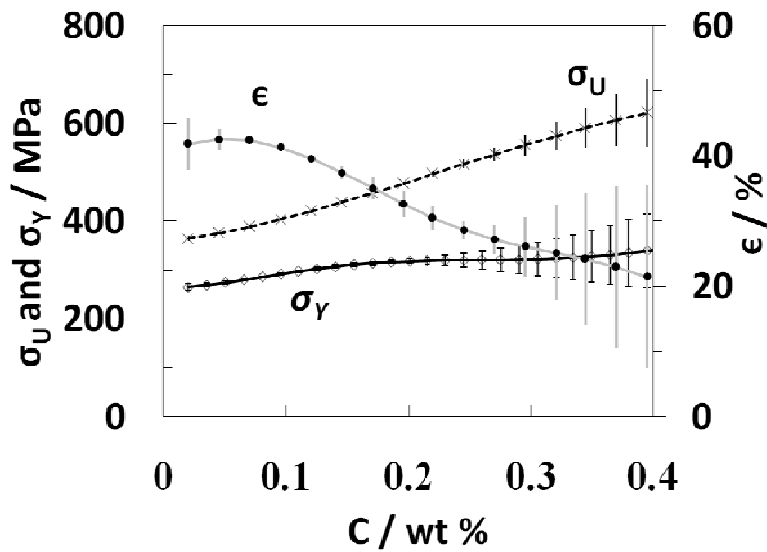

Figure 3.1 Effect of carbon on σ_U, σ_Y and ϵ of alloy A (Table 3.1).
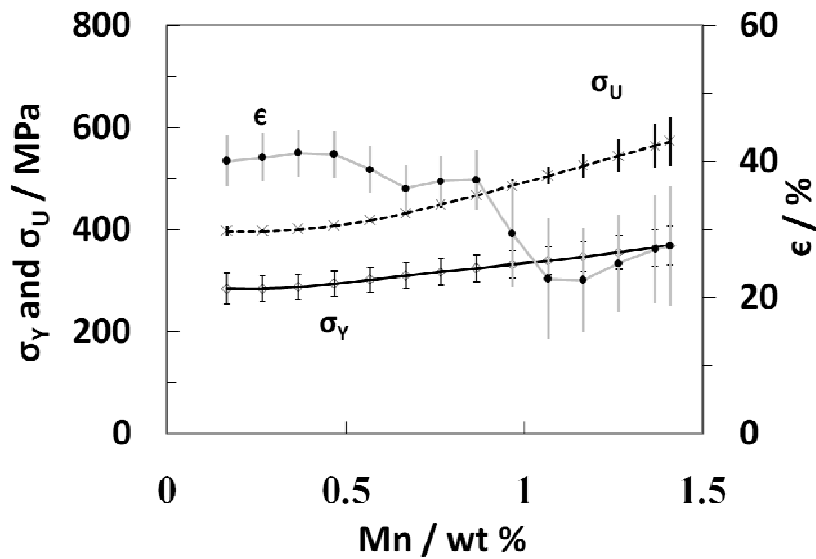
Figure 3.2 Effect of manganese on σ_U, σ_Y and ϵ of alloy A.

Figures 3.3 (a) to (f) show the combined effects of C and Mn contents versus the σ_U, σ_Y and ϵ on the composition A. They show the non-linear relationships that are not captured by the linear regression methods, such as those of Pickering in equations 1-5 and 1-6. The neural network models can capture more complex interactions, but the linear regression will simply be a set of straight lines. C and Mn are principally solid solution strengtheners, and C is in this respect more powerful than Mn. The σ_U calculation for very large carbon concentrations (>0.4 wt %) are too uncertain to draw conclusions (Figure 3.3a and b), but interesting interpretations can be made for carbon concentrations less than 0.4 wt %. For example, the same σ_U can be obtained in Fe-0.2C-0.4Mn wt % and Fe-0.2C-1.4Mn wt % steels. The former steel would be better from a weldability point of view.

48
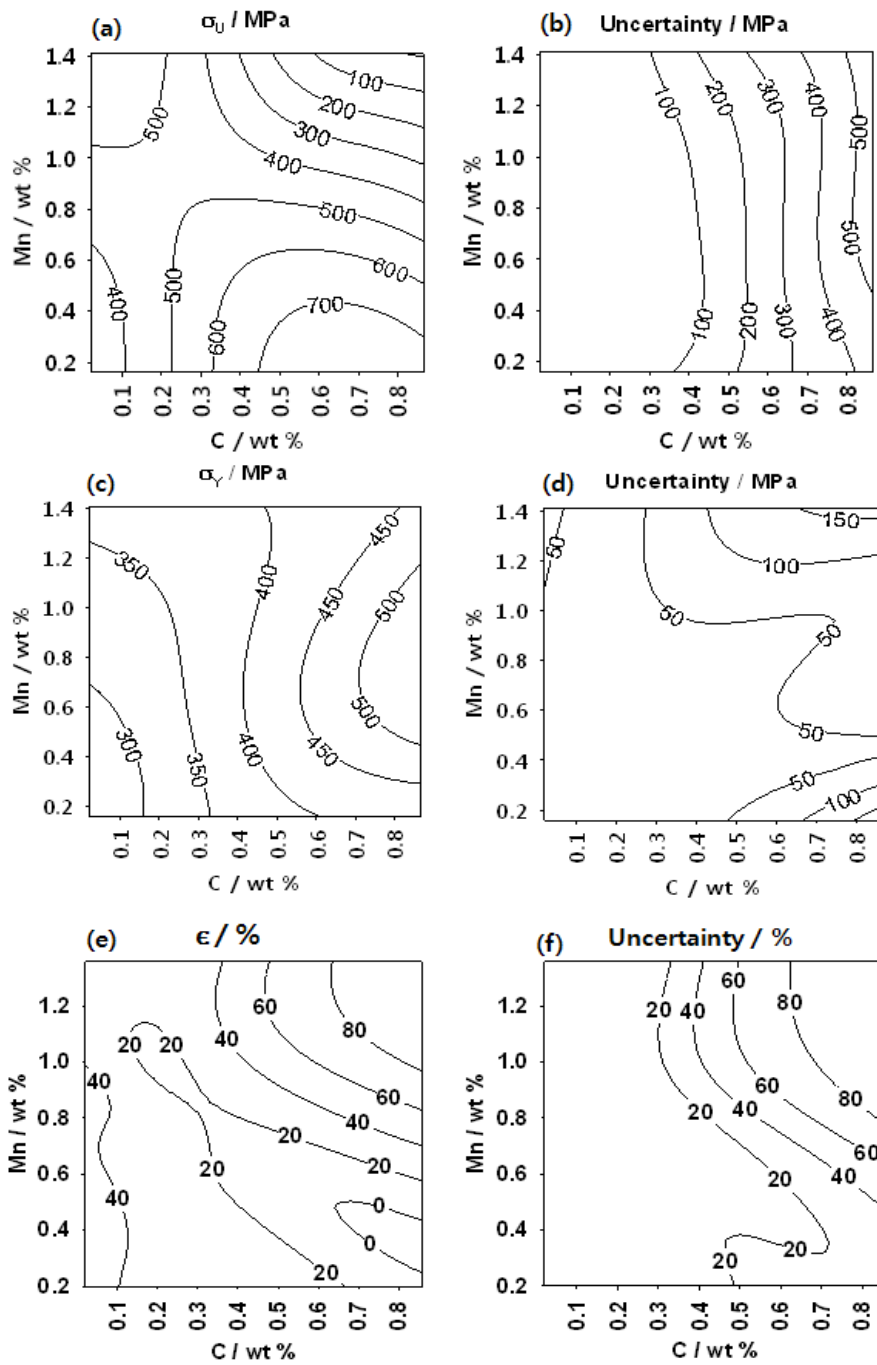
Figure 3.3 (a), (c) and (e): Contour plots of σ_U, σ_Y and ϵ respectively for C versus Mn; (c), (d) and (f) are plots of σ_U, σ_Y and ϵ uncertainty respectively.

49

Figure 3.4 shows the predicted σ_U, σ_Y and ϵ against the Si content for the composition B. The uncertainties are omitted for clarity. The addition of silicon increases σ_U, and probably due to the solid-solution hardening. The predicted ϵ increases about over 1.0 wt % Si, and this is quite consistent with previous study [Tsukatani et al., 1991]. Silicon addition over 1.0 wt % results in a significant increase in the volume fraction of retained austenite and the increment of elongation is attributed to the transformation of retained austenite into martensite during plastic straining and the resultant increase in work-hardening [Bhadeshia and Edmonds, 1980; Tsukatani et al., 1991]. As a result, the product of tensile strength and elongation can be large when the concentration of Si exceed 1 wt %.

Figure 3.4 Effect of silicon on σ_U, σ_Y and ϵ of alloy B.

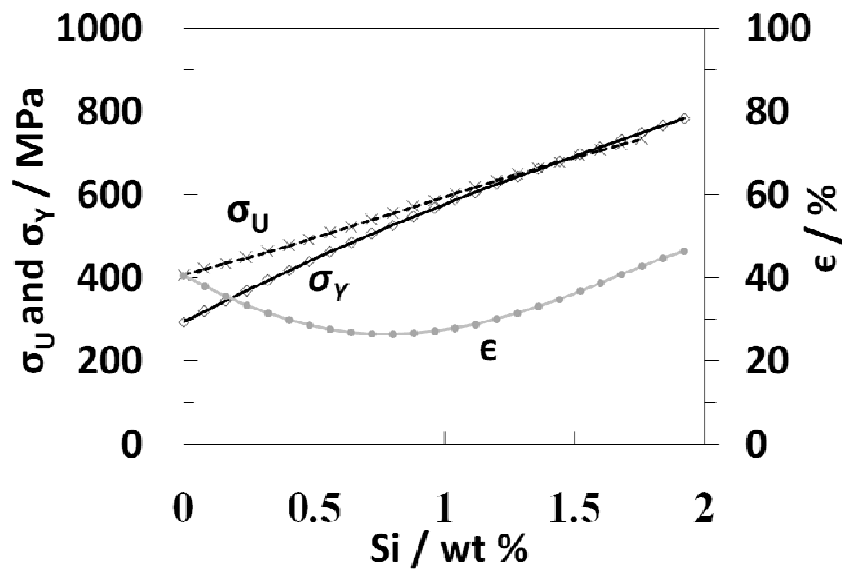## 3.2 Microalloying Elements

Nb, Ti and V carbonitrides prevent austenite grain coarsening during reheating and also help refine the austenite grain size during the hot-rolling process by pinning the grain boundaries and retarding recrystallisation [Amin and Pickering, 1981]. By suppressing recrystallisation, they allow a higher fraction of the strain to be retained in the austenite. This increases the number density of ferrite nucreation sites, and finer ferrite grains are obtained after cooling. Nb is the most effective microalloying addition for suppressing the recrystallisation [Irvine et al., 1967].

Figure 3.5 shows the effect of Nb content on σ_U and σ_Y of alloy C. The measured σ_U and σ_Y are 475 and 430 MPa at 0.023 wt % Nb [Hashimoto, 2003], compared with the predicted values respectively of 466 and 476 MPa for the same alloy. The addition of Nb enhances the σ_Y more than the σ_U. The models show the increases of 46 and 112 MPa for the σ_U and σ_Y respectively on the same amount of Nb (0.023 wt %) increase, whereas the measured increments are respectively 55 and 100 MPa [Hashimoto, 2003].

The addition of Nb also increases the ϵ on the composition C as shown in figure 3.6, because Nb contributes not only to precipitation hardening but also to ferrite grain size refinement associated with the elongation. The prediction results (34 %) at 0.023 wt % of Nb are quite consistent with independently reported data (33 %) [Hashimoto, 2003].
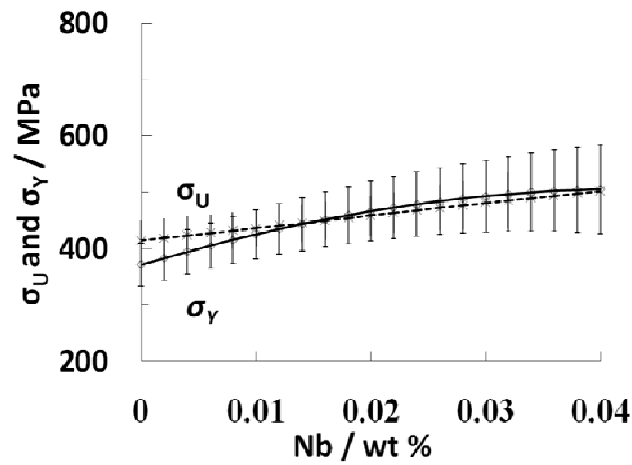
Figure 3.5 Effect of niobium on σ_U and σ_Y of alloy C.
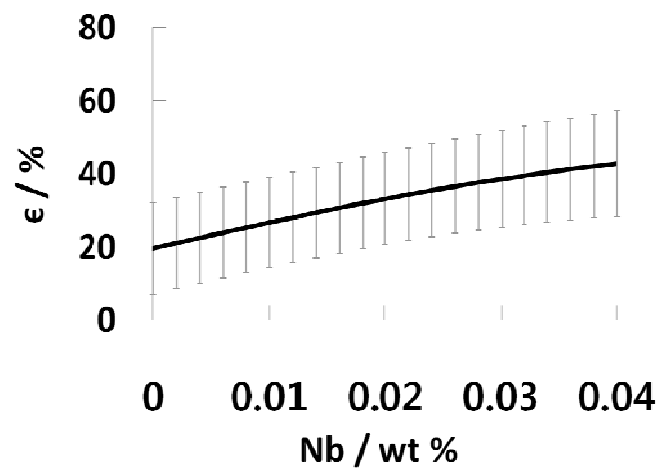
Figure 3.6 Effect of niobium on ϵ of alloy C.

Ti also increases the tensile and yield strength on the composition D [figure 3.7]. The models make good predictions, although they are associated with large modeling uncertainties. The predicted values are 542 and 450 MPa

for σ_U and σ_Y respectively at 0.057 wt%, whereas the measured values are 540 and 480 MPa for the same alloy [Mesplont, 2006]. Ti lead to a reduction in ϵ [figure 3.8], because it contributes more to the precipitation hardening than to the grain refinement.
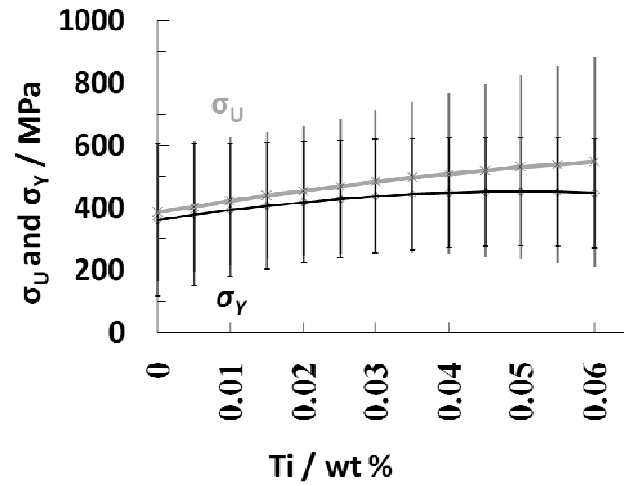
Figure 3.7 Effect of titanium on σ_U and σ_Y for alloy D.
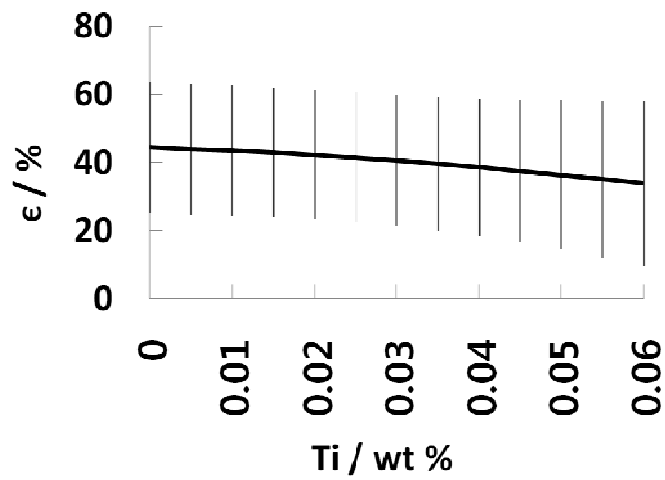
Figure 3.8, Effect of titanium on ϵ of alloy D.

Figures 3.9 to 10 show the contour plots of σ_U and σ_Y for the Nb against V and Nb against Ti on the composition B. These figures show well the complex interactions of these variables.
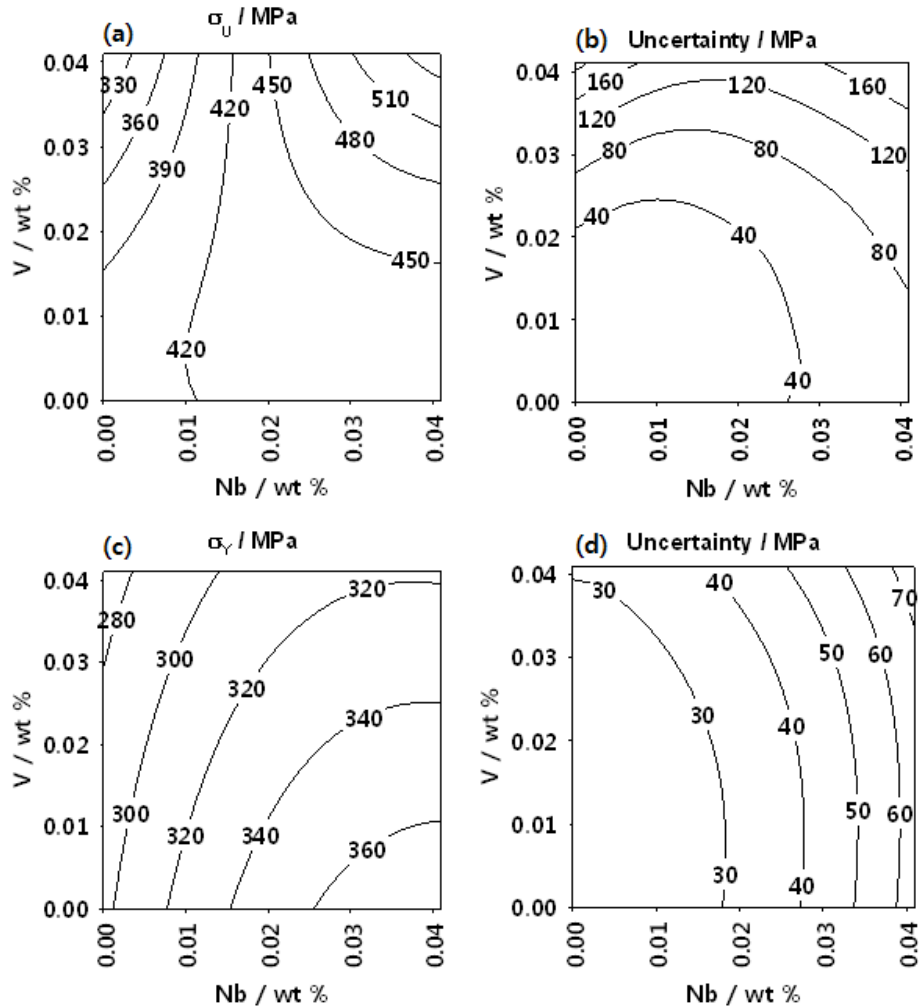
Figure 3.9, (a) and (c): Contour plots of σ_U and σ_Y respectively for Nb versus V of alloy B; (b) and (d) are plots of σ_U and σ_Y uncertainty respectively.
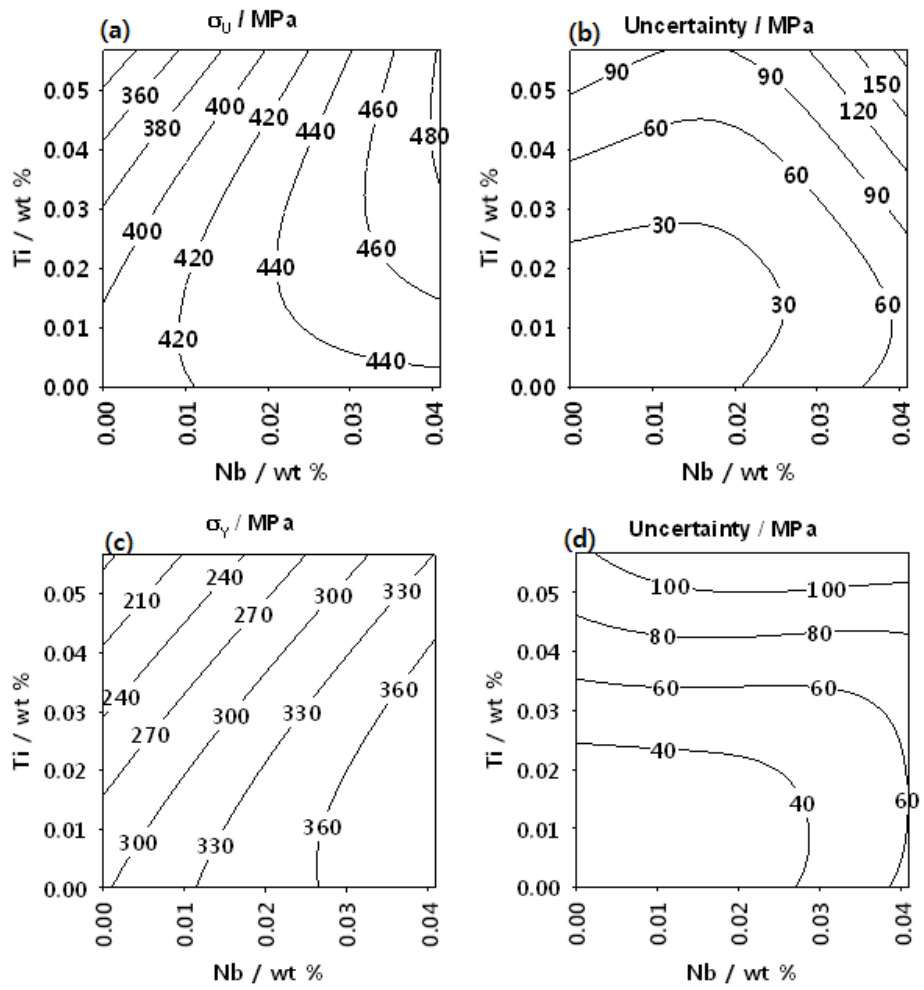
Figure 3.10 (a) and (c): Contour plots of σ_U and σ_Y respectively for Nb versus Ti; (c) and (d) are plots of σ_U and σ_Y uncertainty respectively.

3.3 Thermomechanical Variables

The finishing rolling temperature (T_{FR}) has an influence on the ferrite grain size and mechanical properties. When $T_{FR} < T_{nr}$, pancaked austenite grains containing deformation bands and twins which contribute to ferrite grain size refinement are produced. In addition, for $T_{FR} < Ae_3$ which corresponds to the equilibrium transformation temperature to ferrite from austenite, deformed ferrite, finer recrystallised ferrite and pearlite are formed [Tanaka, 1981]. Consequently, a decrease in T_{FR} enhances the σ_U of alloy B as shown in figure 3.11. The Ae_3 and Ae_1 which is the onset of cementite are calculated using MatCALC, and T_{nr} is calculated using equation 1-14.
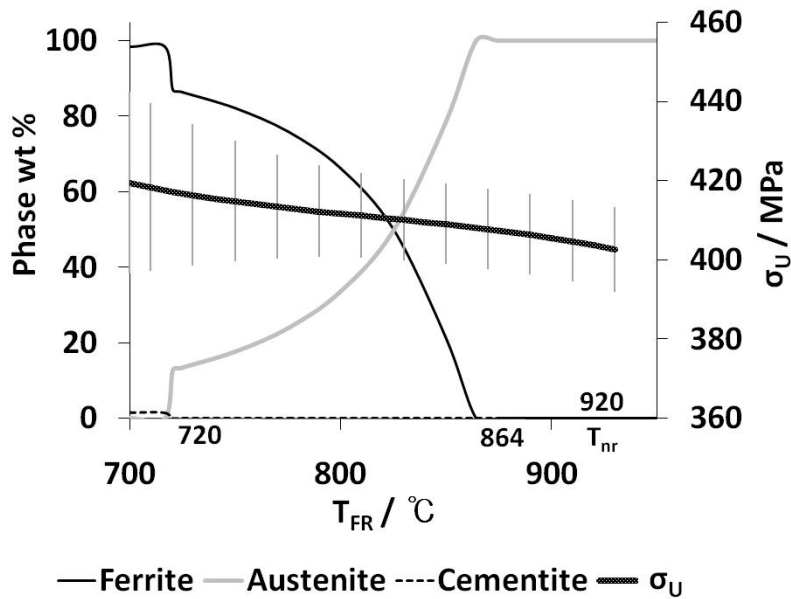
Figure 3.11 Effect of T_{FR} on σ_U of alloy B. Ae_1 is 720 ℃, Ae_3 864 and T_{nr} 920.

Figures 3.12 to 3.14 show effects of the coiling temperature T_C on σ_U, σ_Y and ϵ for alloy E; experimental data correspond to black dots [Zrnik, 2003]. The models show little effects of T_C, however, they give reasonable results for the addition of microalloying. Figure 3.12 shows a light change in σ_U due to the addition of microalloying elements, the increment being less than that for σ_Y as illustrated in figure 3.13.

Figure 3.15 shows the combined effects of T_C and T_{FR} on σ_U for alloy B [figure 3.11]. The maximum difference of the σ_U for the combined variation of the two variables is about 40 MPa. This is because in a steel of this composition, phase transformations are probably completed rapidly, before coiling at the temperature.
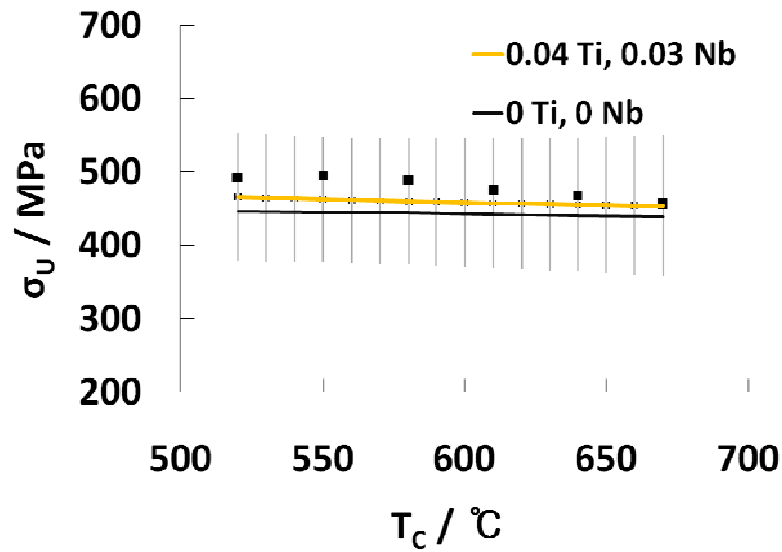
Figure 3.12 Effect of T_C and microalloying elements on σ_U of alloy E.
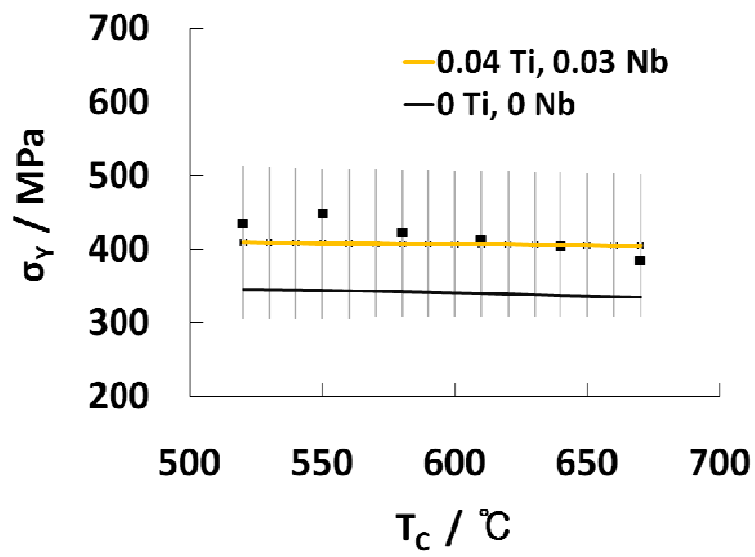
Figure 3.13 Effect of T_C and microalloying elements on σ_Y of alloy E.
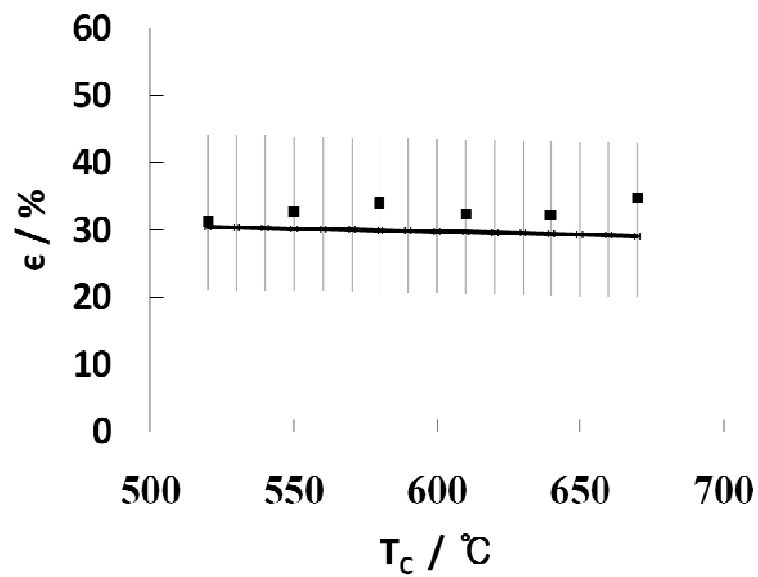
Figure 3.14 Effect of T_C on ϵ of alloy E.

58
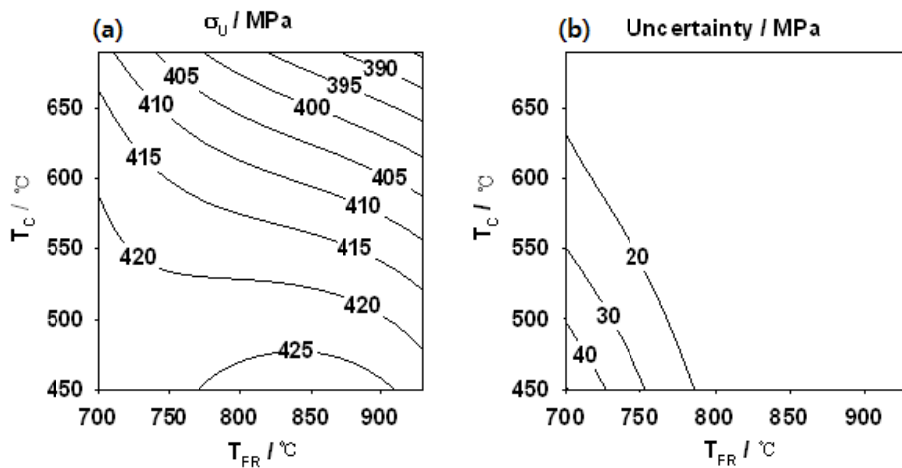
Figure 3.15 (a) Combined effect of T_{FR} and T_C on σ_U of alloy B
(b) uncertainty

The ε_r increases the σ_U and σ_Y on the composition B as shown in figure 3.16, because the larger ε_r contributes more to the grain refinement of the ferrite [Zrnik et al., 2003]. The effect of ε_r to the ϵ is complicated on the same composition, and the large uncertainty is omitted for clarity.
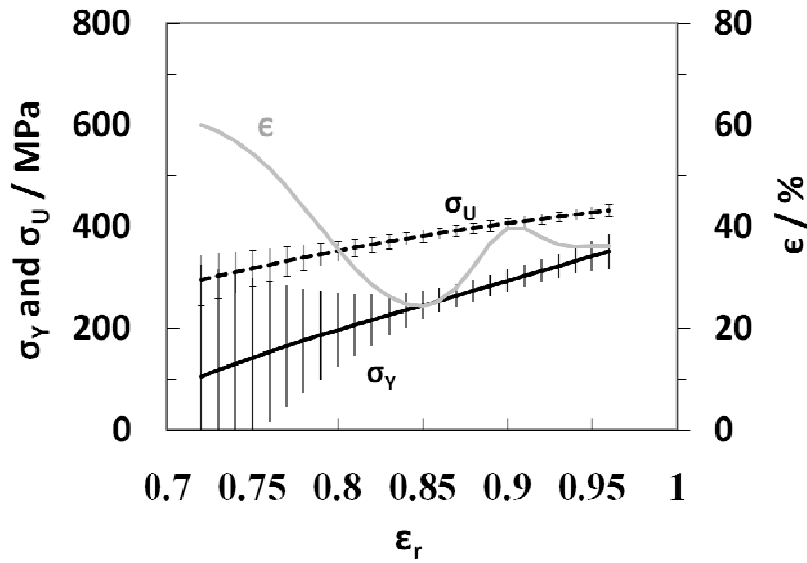
Figure 3.16 Effect of ε_T on σ_U, σ_Y and ϵ of alloy B

3.4 Comparisons between Models

Data for further steels were collected from published results [Panigrahi, 2001; Kim et al, 2000; Hashimoto, 2003; Patel and Wilshire, 2002; Mesplont, 2006; Mitchel, 2005; Barrett and Wilshire, 2002; Xiao et al., 2006; Lee et al., 2002]. Their chemical compositions are described in table 3.2. These experimental results were used to demonstrate the predictive abilities of the neural network models and to make comparisons between models and with linear models. The linear models were trained on the second dataset in the table 2.2, and the weights of variables were determined by minimizing the sum of the residuals (the difference between the predicted and observed values) squared (least square method) [Whittaker, 1967; York, 1966]. The linear models have been produced as follows:

$$\sigma_U \,/\, \text{MPa} = 76.5 + 739W_C + 56.4W_{Mn} + 101W_{Si} + 789W_P - 493W_S + 71.0W_{Cr} + 163W_{Ni} - 86.8W_{Mo} - 182W_{Ti} + 3003W_{Nb} - 63W_V - 11.0W_{Al} + 1481W_N - 2191W_B - 97.3W_{Cu} + 383W_{Sn} + 4630W_{Ca} - 0.0743W_{T_{FR}} - 0.0918W_{T_C} + 0.0282W_{C_t} + 0.00790W_{t_R} - 0.0053W_{T_R} + 362W_{\varepsilon_T}$$

(3-1)

$$\sigma_Y \,/\, \text{MPa} = 56 + 324W_C + 63.3W_{Mn} + 81.5W_{Si} + 688W_P - 1347W_S + 23.9W_{Cr} + 151W_{Ni} + 101W_{Mo} - 274W_{Ti} + 4745W_{Nb} - 879W_V - 51.8W_{Al} + 2629W_N - 3197W_B - 65.9W_{Cu} + 1375W_{Sn} + 13907W_{Ca} - 0.0314W_{T_{FR}} - 0.138W_{T_C} + 0.0706W_{C_t} + 0.00383W_{t_R} - 0.0269W_{T_R} + 690W_{\varepsilon_T}$$

(3-2)

$$\epsilon \,/\, \% = 34.8 - 40.1W_C - 12.3W_{Mn} - 5.42W_{Si} - 166W_P + 75.2W_S + 47.3W_{Cr} - 23.4W_{Ni} - 158W_{Mo} + 17.0W_{Ti} + 102W_{Nb} - 52.4W_V - 38.1W_{Al} - 353W_N - 3725W_B - 0.7W_{Cu} - 83.8W_{Sn} - 530W_{Ca} + 0.0136W_{T_{FR}} - 0.00699W_{T_C} + 0.00205W_{C_t} + 0.00129W_{t_R} + 0.00129W_{T_R} - 5.9W_{\varepsilon_T}$$

(3-3)

where W are the contents of variables in the same units as in table 2.2.

| C	Mn	Si	P	S	Cr	Ni	Mo	Ti	Nb	V	Al	N	B	Cu	Sn	Ca
0.13	0.85	0.073	0.032	0.004	0	0	0	0	0	0	0.03	0.0038	0	0	0	0
0.12	1.34	0.044	0.021	0.001	0	0	0	0	0	0	0.033	0.003	0	0	0	0
0.1	1.2	0.79	0.013	0.001	0	0	0	0	0	0	0.043	0.003	0	0	0	0
0.312	1.51	0.27	0.021	0.008	0	0	0	0	0	0	0.029	0.0031	0	0	0	0
0.1	0.91	0.01	0.011	0.008	0	0	0	0.041	0.031	0.003	0.04	0.007	0	0.029	0	0
0.08	0.8	0.25	0.014	0.011	0	0	0	0	0	0	0.03	0	0	0	0	0
0.08	0.81	0.26	0.013	0.011	0	0	0	0	0.03	0	0.03	0	0	0	0	0
0.08	0.8	0.23	0.012	0.011	0	0	0.3	0	0.03	0	0.03	0	0	0	0	0
0.08	0.8	0.25	0.014	0.011	0	0	0.6	0	0.03	0	0.03	0	0	0	0	0
0.08	0.8	0.25	0.013	0.011	0	0	0.3	0	0	0	0.03	0	0	0	0	0
0.08	0.8	0.26	0.013	0.011	0	0	0.6	0	0	0	0.03	0	0	0	0	0
0.018	0.15	0.01	0.015	0.01	0	0	0	0	0	0	0.05	0.0035	0	0	0	0
0.0026	0.17	0	0.011	0.011	0	0	0	0.053	0	0	0.06	0.0013	0	0.008	0	0
0.0026	0.17	0	0.011	0.011	0	0	0	0.053	0	0	0.06	0.0013	0	0.008	0	0
0.025	1.56	0.24	0.002	0.0006	0	0	0.32	0	0.039	0.019	0	0.0062	0	0	0	0
0.049	1.45	0.51	0.014	0.002	0	0	0	0	0.025	0	0.047	0.0094	0	0	0	0
0.1	1.5	0.35	0	0.005	0	0	0	0	0	0.03	0.025	0.006	0	0	0	0
0.057	0.53	0	0	0	0	0	0	0	0	0	0.044	0.0046	0	0	0	0
0.052	0.52	0	0	0	0	0	0	0	0.019	0	0.035	0.0053	0	0	0	0
0.05	0.52	0	0	0	0	0	0	0	0.05	0	0.027	0.0053	0	0	0	0
0.055	0.52	0	0	0	0	0	0	0.019	0.052	0	0.046	0.0054	0	0	0	0
0.057	0.54	0	0	0	0	0	0	0.025	0.054	0	0.05	0.0062	0	0	0	0
0.058	0.52	0	0	0	0	0	0	0.057	0.054	0	0.052	0.0088	0	0	0	0
0.073	1.36	0	0	0.003	0	0	0	0	0.068	0	0.045	0.006	0	0	0	0
0.19	1.53	1.44	0	0	0	0	0	0	0	0	0	0	0	0.51	0	0
0.18	1.56	1.53	0	0	0.36	0	0	0	0	0	0	0	0	0.51	0	0
0.21	1.43	1.43	0	0	0	0.43	0	0	0	0	0	0	0	0.51	0	0
0.2	1.43	1.43	0	0	0.4	0.42	0	0	0	0	0	0	0	0.51	0	0

Table 3.2: Chemical compositions (wt %) to demonstrate the predictability of models. The details of rolling schedule for the calculation are assumed to be the same as the mean values used here if they were missing in the literature.

Figures 3.17a to d show plots of the measured values versus predicted values for σ_U, e to h for σ_U and i to m for the ϵ of the alloys in the table 3.1. The neural network models trained on the first dataset show large uncertainties and rough predictions for these alloys as shown in the figures 3.17a, e and i. On the other hand, the neural network models trained on the second dataset give more acceptable results (figures 3.17b, c, f, g, j, k and l). It confirms that a few cases which are solute-rich on the second dataset can raise the predictive power of the models and reduce the uncertainties. In addition, the prediction results of the models which include 23 input variables (figures

3.17c, g and l) are more compatible with the experimental results than those of the models that trained on the same dataset, but consist of 19 variables (figures 3.17b, f and j). In the case of ϵ models, the natural logarithm functional of equation 2-2 contribute to the better predictions as shown in the figure 3.17l, compared to the figures 3.17k. The prediction results of linear models are also compared with experimental results in the figure 3.17d, h and m.
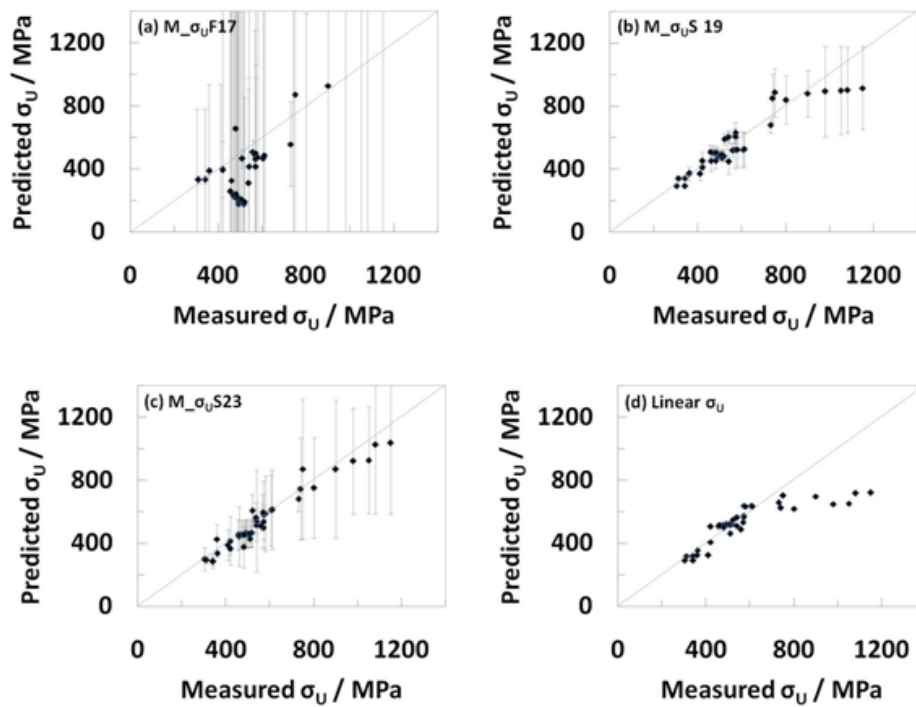
(a) Neural network model trained on the first dataset consisting of 17 input variables for σ_U.
(b) Neural network model, second dataset, 19 input variables, σ_U.
(c) Neural network model, second dataset, 23 input variables, σ_U.
(d) Linear model, second dataset, 23 input variables, σ_U.

(e) Neural network model trained on the first dataset consisting of of 17 input variables for σ_Y.

(f) Neural network model, second dataset, 19 input variables, σ_Y.

(g) Neural network model, second dataset, 23 input variables, σ_Y.

(h) Linear model, second dataset, 23 input variables, σ_Y.
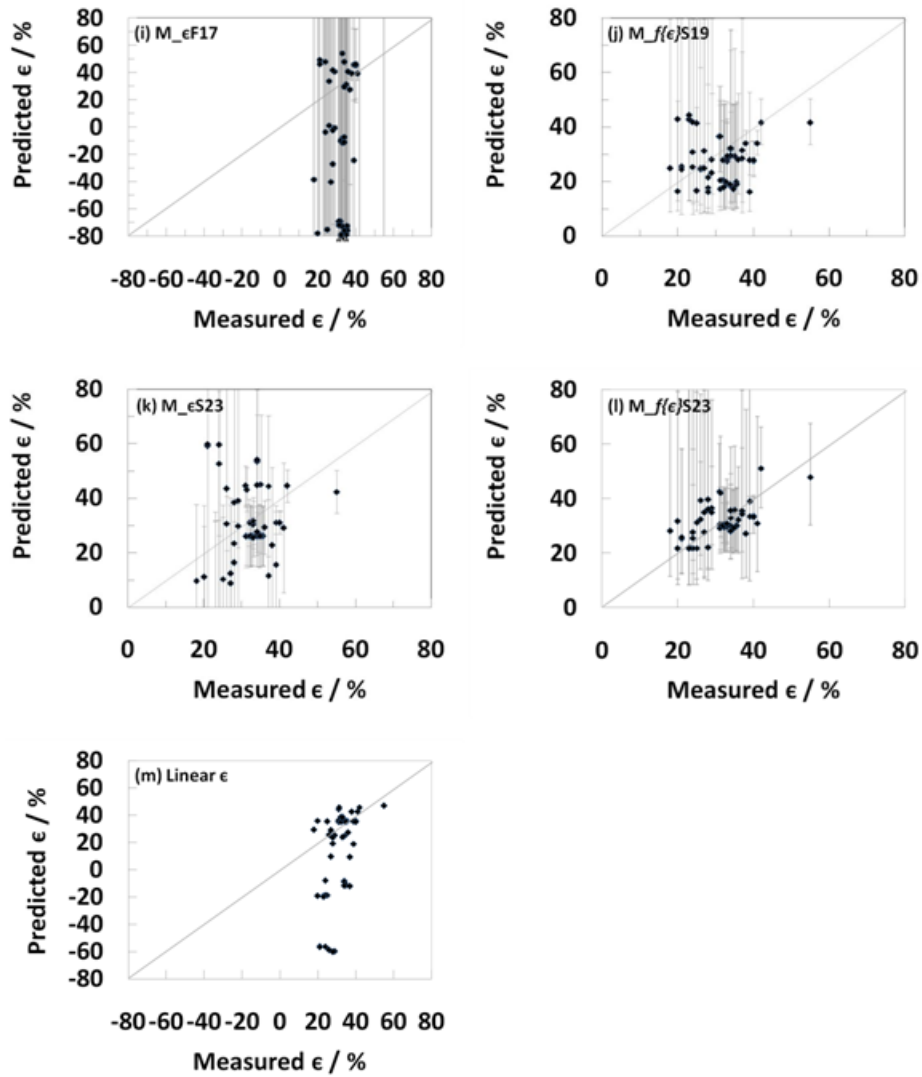
(i) Neural network model trained on the first dataset. Number of input variables is 17, and function of output is directly ϵ.
(j) Neural network model, second dataset, 19 input variables, $f\{\epsilon\}$.
(k) Neural network model, second dataset, 23 input variables, ϵ.
(l)   Neural network model, second dataset, 23 input variables, $f\{\epsilon\}$.
(m) Linear model, second dataset, 23 input variables, ϵ.
Figure 3.17 Measured values versus predicted values.

3.5 Summary

Several neural network models have been produced to make a comparison between models. The models were used to demonstrate some of the trends that are predicted from the models by varying the contents of one variable and keeping other contents constant. The carbon, manganese, silicon and microalloying elements (Nb, Ti, V) increase the σ_U and σ_Y, however the trends depend on the position in the input space. The combined effects of two variables, therefore, have been described by the contour plots. The effect of thermomechanical variables also has been studied. The increase of C_t and ε_T show the strengthening effect, but T_{FR} and T_C give little effect. The variables, in general, give more complicated effects to the ϵ than the σ_U and σ_Y.

The comparisons between the models which have a same output show an effect of input space and number of inputs. The uncertainty depends a lot on the input space and the predicted values of the model which has more variables and wider input space are more compatible to the experimental results. The predicted values of neural network models and linear models have been compared with further published data. The natural logarithm functional has been used to avoid negative predictions, thus making better prediction. However, it should be noted that the natural logarithm functional may unnecessarily bias or constrain the analysis - it should almost be regarded as an intervention.

IV Future Work

It has been demonstrated in the present work that sophisticated problems such as the properties of hot-rolled steels can be quantitatively modeled using the neural network method. Interesting trends have been revealed and some of the phenomena could be usefully explored using experiments. For example, it seems possible to produce identical mechanical properties for different compositions, leaving the possibility of reducing grades and hence improving profitability. In spite of all the successes, it has to be recognised that the modeling of properties is in its infancy. The section below therefore sets out the scene for the future work.

In the field of modeling, tremendous progress has been made on all aspects and levels of microstructure and phase stabilities. However, a major unexplored area is the creation of generally applicable models for complex mechanical properties. For example, if a user has the comprehensive detail of microstructure, chemical composition and processing for all arbitrary steel, it is not possible to calculate plasticity, fatigue, toughness or creep behavior. A huge amount of work has been done to measure mechanical properties and to use them in safe design, but not in predicting these properties except in very narrow classes of steels using empirical methods.

In future work, it is intended to begin the creation of fundamental algorithms which are generally applicable, for these properties. For example, it should be possible to formulate an algorithm for the strength of pure, annealed iron (without any microstructure) as a function of temp and strain rate. This would represent the base strength of any steel. It would then be possible to build on this to include other phenomena such as solution effects etc.

References

Amin, R. K. and Pickering F. B., Thermomechanical Processing of microalloyed austenite, ed. DeAdro, A. J. et al., 1; Warrendale, TMS-AIME, 1981

Barrett, C. J. and Wilshire, B., The production of ferritically hot rolled interstitial-free steel on a modern hot strip mill, *Journal of Materials Processing Technology*, 122: 56-62, 2002

Bhadeshia, H. K. D. H., and Edmonds, D. V., Analysis of the Mechanical Properties and Microstructure of a High-Silicon Dual-Phase Steels, *Metal Science,* 14: 41-49, 1980

Bhadeshia, H. K. D. H., Neural Networks in Material Science, *ISIJ Intenational*, 39: 966-979, 1999.

Bhadeshia, H. K. D. H. and Sourmail, T., Neural Networks, *Introduction to Materials Modelling*, ed. Zoe Barber, Institute of Materials, London, 2003

Bhadeshia, H. K. D. H., The Importance of Uncertainty, *Neural Networks and Genetic Algorithms in Materials Science and Engineering*, Tata McGraw-Hill Publishing Company, Bengal Engineering and Science University, India, 2006.

Bleck, W., Meyer, L. and Kasper, R., *Stahl u. Eisen,* 110: 26, 1990.

Boratto, F., Barbosa, R., Yue, S. and Jonas, J. J., Effect of Chemical Composition on the
Critical Temperatures of Microalloyed Steels, THERMEC ´88. Proceedings. ed. Tamura, I. (Tokyo: Iron and Steel Ins.), 383-390, 1988.

Bramfit, B. L. and Marder, A. R., Processing and properties of low carbon steels, *AIME*, 191, 1973.

Cottrell, A. H., Dislocations and Plastic Flow in Crystals, Oxford University Press, London, 1953

Cuddy, L. J., Encyclopedia of materials science and engineering, Oxford, Pergamon, 1985.

Cuddy, L. J., The Effect of Microalloy Concentration on the Recrystallization of Autenite During Hot Deformation*, Thermomechanical Processing of Microalloyed Austenite*, 129-140. 1982.

Cohen, M. and Hansen H. H., HSLA steels: Metallurgy and apllcation, ed. Gray, J. M., et al., Metals Park, OH, ASM, 61, 1986,.

DeAdro, A. J., *Conference high strength low alloy steels,* ed. Dunne, D. P. and Chandra, T., Wollongong: Unversity of Wollongong, 70, 1984.

Dieter, G. E., Mechanical Metallurgy SI Metric Edition, McGraw Hill, London, 307−308, 1988

Doherty, R. D., Hughes, D. A., Humphreys, F. J., Jonas, J. J., Jensen, D. J., Kassner, M. E.,   King, W. E., McNelley, T. R., McQueen, H. J. and Rollett, A. D., Current Issues in Recrystallization*, Materials Science and Engineering A*, 238: 219-274, 1997.

Eastering, K., Physical metallurgy of welding, London, Butterworth, 122, 1992.

Ferry, P. M. and Chandra, T., Five Decades of the Zener Equation, *ISIJ International*, 38: 913-924, 1998.

Felbeck, D. K. and Atkins, A. G., Strength and Fracture of Engineering Solids, Prentice-Hall Inc., 1984.

Gladman, T., The Physical Metallurgy of Microalloyed Steels, The institute of materials, London, 1997

Hansen, S. S., Vander Sande, J. B. and Cohen, *Met. Trans.* A11: 387-402, 1980

Honeycombe, R. W. K., The Plastic Deformation of Metals, Edward Arnold, 1968

Honeycombe, R. W. K., Steels – Microstructure and Properties, Edward, Arnold, 1981

Hashimoto, S., Effect of Nb on Hot Rolled High Strength Steel Sheets Produced by Thin Slab Casting and Hot Direct Rolling Process, *ISIJ International*, 43: 1658–1663, 2003

Hensel, A. and Lehnert, L., *neue hutte*, 18: 654, 1973.

Hodgson, P. D., Models of the recrystallisation behaviour of C-Mn and Nb microalloyed steels during hot working processes, *Material Forum*, 17: 403-408, 1993.

Hoile, S., Processing and properties of mild interstitial free steels, *Material Science and Technoogy*, 16: 1079-1093, 2000.

Irvine, K. J., Pickering, F. B., Gladman, T., *Grain-Refined C-Mn Steels*, *Journal of the Iron and Steel Institute*, 210: 161, 1967

Jaiswal, S. and McIvor, I. D., *Ironmaking and Steelmaking*, 16: 49, 1989.

Jianlin, Xu, A Genetic Neural Network for Predicting Materials Mechanical Properties, *Third International Conference on Natural Computation (ICNC 2007)*, l: 710-714. 2007

Kim, S. J., Chang, G. L., Lee, T. H. and Lee, S. H., Effects of Coiling Temperature on Microstructure and Mechanical Properties of High-strength Hot-rolled Steel Plates Containing Cu, Cr and Ni, *ISIJ International*, 40: 692–698, 2000

LeBong, A. and Rofez Vernis, J., *Conference controlled processing of HSLA steels*, York, UK: University of York, paper no. 6, 1976.

Lee, W. B., Hong, S. G., Park, C. G. and Park, S. H., Carbide Precipitation and High-Temperature Strength of Hot-rolled High-Strength, Low-Alloy Steels Containing Nb and Mo, *Metallurgical and Materials Transaction A*, 33A:1689, 2002

MacKay, D. J. C., Bayesian interpolation, *Neural Computation*, 4: 415-447, 1992.

MacKay, D. J. C., Practical bayesian framework of backpropagation networks, *Neural Computation*, 4: 448-472, 1992.

MacKay, D. J. C., Bayesian non-linear modelling with neural networks, University of Cambridge programme for industry: modelling phase transformations in stels, 1995

MacKay, D. J. C., Probability theory and Occam's razor, *Darwin College Magazine*, 81-85, 1993.

MacKay, D. J. C., Probability theory and Occam's razor, Mathematical Modeling of Weld Phenomena III, *The Institute of Materials*, London, 359-389, 1997.

Martin, S., Bjorn, F., Bernhard, L., Thomas, P. and Thomas, R., Neural computation in steel industry, *Proceeding of the Euopean control conference'99*, 1999

Medina, S. F., Microstructural Modeling for Low Alloy and Microalloyed Steels, 2nd *International Conference on Modeling of Metal Rolling Process*, 501-510, 1996.

Mesplont, C., Grain refinement and high precipitation hardening by combining microalloying and accelerated cooling, *Revue de Métallurgie,* 238-246, 2006

Mitchell, P. S., The Development of Vanadium Containing Steels Suitable for Thin Slab Casting, Materials Science Forum, 500-501: 269-279, 2005

Morrison, W. B., The effect of grain size on the stress-strain relationship in low carbon steel, *Trans. ASM*, 59:824-846, 1966

Nolle, L., Armstrong, A., Hopgood, A. and Ware, A., Optimum work roll profile selection in the hot rolling of wide steel strip using computational intelligence, Lecture Notes in Computer Science, 1625: 435-452, 1999

Ouchi, C., Sanpei, T., Okita, T. and Kozasu, I., Microstructural Change of Austenite During Hot Rolling and Their Effent of on Transformation Kinetics, *AIME*, 316-340, 1977.

Panigrahi, B. K., Processing of low carbon steel plate and hot strip—an overview, *Bull. Mater. Sci.*, 24: 361–371, 2001

Patel, J. K. and Wilshire, B., The challenge to produce consistent mechanical properties in Nb-HSLA strip steels, *Journal of Materials Processing Technology,* 120: 316–321, 2002

Perry, A. C., Thompson, S. W. and Speer, J. G., Physical metallurgy of ferritic hot rolled low carbon steel, *Iron & Steel Maker,* 27: 47-57, 2000.

Pickering, F. B., Physical Metallurgy and the Design of Steels, *Applied Science Publishers*, London, 50, 1978.

Priestner, R. and de Los Ris, E., *Heat Treatment '76*, London: Metals Soc., 129, 1976.

Richard, C., Grain Sizes of Ceramics by Automatic Image Analysis, *Journal of the American Ceramic Society*, 77: 589, 1994

Sakir, B., Effect of Pearlite Banding on Mechanical Properties of Hot-rolled Steel Plates, *ISIJ international*, 31: 1445-1446, 1991

Shimizu, M., Hiromatsu, M., Takashima S., Kaji, H., ad Kano, M. HSLA steel: metallurgy and applicaton, ed. Gray, J. M., et al., Metal Park, OH, ASM, 591,1986

Singh, S., Bhadeshia, H. k. D. H., MacKay, D., Carey, H. and Martin, I., Neural network analysis of steel plate processing, *Ironmaking and Steelmaking*, 25: 355-365, 1998.

Taylor, G. I., Mechanism of plastic deformation of crystals, *Proc. Roy. Soc.,* A145, 362, 1934

Tamura, I., Sekine, H., Tanaka, T. and Ouchi, C., Thermomechanical Processing of High Strength Low Alloy Steels, *Butterworths*, London, 1988.

Tanaka, T., *Conference high strength low alloy steels,* ed. D. P. Dunne and Chandra, T., Wollongong: University of Wollongong, 6, 1984.

Tanaka, T., *Int. Met*. Rev., 26: 185, 1981.

Tomitz, A. and Kaspar, R., *Steel Res.,* 71: 233, 2000.

Tsukatani, I., Hasimoto, S. and Inoue, T., Effect of Silicon and Manganese Addition on Mechanical Properties of High-Strength Hot-Rolled Sheet Steel Containing Retained Austenite, *ISIJ international*, 31:992-1000, 1991
Underwood, E., *Quantitative streology*, NY: Addison Wesley, 1970.

Warde, J. and Knowles, D. M., Application of Neural Networks to Mechanical Property Determination of Ni-base Superalloys, *ISIJ International*, 39: 1006-1014, 1999.

Whittaker, E. T. and Robinson, G., The Method of Least Squares, Ch. 9 in The Calculus of Observations: A Treatise on Numerical Mathematics, 4th ed. New York: Dover, 209, 1967.

Xiao, F. R., Liao, B., Shan, Y. Y., Qiao, G. Y., Zhong, Y., Zhang, C. and Yang, K., Challenge of mechanical properties of an acicular ferrite pipeline steel, *Materials Science and Engineering A*, 431: 41–52, 2006

York, D., Least-Square Fitting of a Straight Line, *Canad. J. Phys.,* 44: 1079-1086, 1966.

Zhu, M. H., Zhao, Y. G., Cai, W., Wu, X. S., Gao, S. N., Wang, K., Luo, L. B., Huang, H. S. and Lu, L., Spin-glass shel and magnetotransport properties of a La$_{0.67}$Ca$_{0.33}$MnO$_3$ nanoring network*, PHYSICAL REVIEW B*, 75, 2007

Zrnik, J., Kvackaj, T., Sripinproach, D. and Sricharoenchai, P., Influence of plastic deformation condition on structure evolution in Nb-Ti microalloyed steel, *Journal of Materials Processing Technology*, 133: 236–242, 2003.

Appendix

This is the documentation for the all models in this work.

**Program
MAP_NEURAL_HOTROLLEDSTEEL_MECHNICALPROPERTIES**

1. Provenance
2. Purpose
3. Specification
4. Description
5. References
6. Parameter
7. Error indicators
8. Accuracy estimate
9. Further comments
10. Example
11. Auxiliary routines
12. Keywords

1 Provenance of Source Code

Joo Hyun Ryu and H. K. D. H. Bhadeshia
Graduate Institute of Ferrous Technology (GIFT)
Pohang University of Science and Technology
Pohang, Kyungbuk, Republic of Korea
windhair@postech.ac.kr

2 Purpose

To estimate the ultimate tensile strength, yield strength and elongation of hot-rolled steels as a function of chemical compositions and thermo-mechanical variables.

3 Specification

Language: FORTRAN and C
Product form: Executables
Complete program

4 Description

In the present work the ultimate tensile strength, yield strength and elongation of hot-rolled steels are predicted as a dependent variable on chemical composition and thermo-mechanical variables. The modeling is based on a neural network with the Bayesian framework.

The program runs on a UNIX operating system and Linux.
The files for UNIX are separated compressed into a file called
mp_hrs.tar

The .tar file contains the following ten directories:
M_UF17, M_YF17, M_EF17, M_US19, M_YS19, M_fES19, M_US23, M_YS23, M_ES23, M_fES23 which are directories of the models described in table 2.3.

Each of directories includes the following files:

readme.txt
This file contains all the relevant information regarding the model such as, the number of data used, the input variables used, explanations on how to run the model and get the desired results.

MINMAX

This file contains the range of the data, its mean and standard deviation of input variables.

test.dat

An input text file containing the input variables used for predictions.

run_model.gen

This is the shell command to be run on the terminal. This command takes the input from the test.dat and runs the model for the given input.

result

Contains the final un-normalised committee results for the predicted output.

Subdirectory C

_w*f   The weights files for the different models
*.lu   Files containing information for calculating the size of the error
            bars for the different models
_c*   Files containing information about the perceived significance value
            for each model
_R*   Files containing values for the noise, test error and log predictive
            error for each model

Subdirectory D

- outran.x   A normalized output file which was created during the building of the model

Subdirectory outprdt
- com.dat   The normalized output file containing the committee results

Detailed instructions on the use of the program are given in the **readme** file*.*

5 References

Singh, S., Bhadeshia, H. k. D. H., MacKay, D., Carey, H. and Martin, I., Neural network analysis of steel plate processing, *Ironmaking and Steelmaking*, 25: 355-365, 1998.

6 Parameters

Input parameters
The input variables for the model are listed in the **readme** file in the corresponding directory. The maximum and minimum values for each variable are given in the file **MINMAX**.

Output parameters
These programs give the tensile and yield strength in MPa, and elongation in percent. The corresponding output is in **result** file. The format of the **result** file is:

Prediction   Error   Prediction-Error   Prediction+Error

7 Error Indicators
None.

8 Accuracy

The uncertainty in predictions is given as a predicted-error and predicted+error

9 Further Comments

Refer to the website to use model manager for making a model.
HTTP://www.neuromat.com

10 Example

10.1 Download the model
Uncompress the "*mp_hrs.tar*" file in a dedicated directory On UNIX systems
     gzip -d mp_hrs.tar
     tar -xvf mp_hrs.tar

10.2 Input data
– for example, effect of carbon to the strength and elongation when the number of input variables is 23.

0.1 0.4 0.2 0 0 0 0 0 0 0 0 0 0 0 0 0 0 0 700 600 350 200 1100 0.9
0.2 0.4 0.2 0 0 0 0 0 0 0 0 0 0 0 0 0 0 0 700 600 350 200 1100 0.9
0.3 0.4 0.2 0 0 0 0 0 0 0 0 0 0 0 0 0 0 0 700 600 350 200 1100 0.9

Each number corresponds to a particular input variable and the details of the input variables are given in the readme.txt file of each model.

10.3 Running the program
Type *sh model.gen*

10.4 Results of the program
The results are written in the "Result" file.

Ultimate tensile strength / MPa

Prediction	Error	Prediction-Error	Prediction+Error
447.332672	34.480125	412.852539	481.812805
516.393311	39.693214	476.700134	556.086548
587.794312	50.716984	537.077332	638.511292

Yield strength / MPa

Prediction	Error	Prediction-Error	Prediction+Error
351.074005	29.272312	321.801727	380.346313
398.154297	29.423172	368.731140	427.577484
437.658081	30.295145	407.362946	467.953217

Elongation

M_ES23

Prediction	Error	Prediction-Error	Prediction+Error
33.278599	7.864700	25.413900	41.143299
32.408192	4.767370	27.640818	37.175564
34.220150	12.371532	21.848618	46.591682

M_fES23

Prediction	Error	Prediction-Error	Prediction+Error
-0.835736	0.858373	-1.694110	0.022637
-1.071533	0.708306	-1.779839	-0.363228
-1.299421	0.581031	-1.880452	-0.718391

Output values of elongation should be converted to original values when the natural logarithm functional is used for the output by following equation:

Elongation / % = (1-EXP(-EXP(Prediction)))*(80-8)+8

11. Auxiliary Routines
None

12. Keywords
neural network, tensile strength, yield strength, elongation, hot rolled steel

Acknowledgements

CURRICULUM VITAE

Name: Ryu, Joo Hyun (柳朱炫)

Date of birth: 14th April, 1980

Place of birth: Jeonnam province, South Korea

Address: 4-405, Graduate Apt., POSTECH,

Hyoja-Dong, Nam-Gu, Pohang,

Kyungbuk, 790-784, South Korea

Education:

M. S. 2008, POSTECH (Pohang, Korea), Graduate Institute of Ferrous Technology, Computational Metallurgy.

B. S. 2006, POSTECH (Pohang, Korea), Department of Chemical Engineering

Parts of this work have been submitted to appear in the following publications.

Ryu, J. H. and Bhadeshia, H. K. D. H., Contribution of Microalloying to the Strength of Hot-rolled Steels, submitted to *Materials and Manufacturing Processes*

Joo, M. S., Ryu, J. H. and Bhadeshia, H. K. D. H., Domains of Steels with Identical Properties, submitted to *Materials and Manufacturing Processes*

Bhadeshia, H. K. D. H., Dimitriu, R., Forsik, S., Pak, J. H. and Ryu, J. H., On the Performance of Neural Networks in Materials Science, submitted to *Materials and Technology.*